STUDIES ON III-V DILUTE NITRIDE, BISMUTH AND ANTIMONIDE ALLOYS USING K.P HAMILTONIAN

Dissertation

Submitted in partial fulfillment of the requirements
for the award of the degree of

Master of Technology

In

Mobile Communication And Computing

By

Indranil Mal

(MCC/15/05)

Under the supervision of:

Dr. T. D. Das

Assistant Professor

Department of Basic and Applied Science

Department of Electronics and Computer Engineering

National Institute of Technology

(Established by Ministry of Human Resource Development, Govt. of India)

Yupia, District: Papum Pare, Arunachal Pradesh 791 112

May 2017

National Institute of Technology
(Established by Ministry of Human Resource Development, Govt. of India)
Yupia, District : Papum Pare, Arunachal Pradesh 791 112
Phone : 0360-2001581 (O), 0360-2001583 (R), Fax : 0360-2284972,
Email : directornitap@gmail.com, Web-site : http://www.nitap.ac.in

CERTIFICATE OF APPROVAL

The dissertation entitled " ***STUDIES ON III-V DILUTE NITRIDE, BISMUTH AND ANTIMONIDE ALLOYS USING K.P HAMILTONIAN"*** submitted by **Indranil Mal** bearing Roll No **MCC/15/05** is presented in a satisfactory manner to warrant its acceptance as a pre-requisite for the degree of Master of Technology in Mobile Communication and Computing of National Institute of Technology, Arunachal Pradesh. It is understood that by this approval the undersigned do not necessarily endorse or approve any statement made, the opinion expressed or conclusion drawn therein, but only for the purpose for which it has been submitted.

BOARD OF EXAMINERS:

1. External Examiner

2. Internal Examiner

National Institute of Technology
(Established by Ministry of Human Resource Development, Govt. of India)
Yupia, District : Papum Pare, Arunachal Pradesh 791 112
Phone : 0360-2001581 (O), 0360-2001583 (R), Fax : 0360-2284972,
Email : directornitap@gmail.com, Web-site : http://www.nitap.ac.in

CERTIFICATE FROM SUPERVISOR

This is to certify that the dissertation entitled "***STUDIES ON III-V DILUTE NITRIDE, BISMUTH AND ANTIMONIDE ALLOYS USING K.P HAMILTONIAN "*** submitted by **Indranil Mal** bearing Roll No. **MCC/15/05** to the Department of Electronics and Computer Engineering of National Institute of Technology, Arunachal Pradesh, as a partial fulfillment of his M.Tech. degree in Mobile Communication and Computing of the Institute is absolutely based upon his own work, carried out during the period from July 2016 to May 2017 under my supervision. Neither this dissertation nor any part of it has been submitted for the award of any other degree of this Institute or any other Institute/ University.

Dr. T. D. Das
Supervisor

ABSTRACT

The electronic band structure of strained GaSbBi/GaAs heterostructures are investigated using a 14 band **k·p** Hamiltonian which is an extended form of the 12 band Valance band Anticrossing (VBAC) matrix. The shift in the valence and conduction subbands due to the incorporation of Bi in GaSb/GaAs Type II system are calculated and compared with the available experimental data. Unlike the band gap reduction of 51 meV and enhancement of spin-orbit splitting energy by ~ 27 meV in bulk $GaSb_{0.987}Bi_{0.013}$, 7.3% compressive strain in GaSbBi/GaAs quantum wells (QWs) amends the scenario completely by increasing the band gap to 1.12 eV and the spin-orbit splitting energy to 1.217 eV. The dispersion relations and effective masses of the carriers in the crystal directions Δ, Λ, and Σ are calculated near the Γ point using this Hamiltonian yield some interesting results. The variation of the optical gain with the density of injected carriers and dimension of the QW is calculated and the peak of the gain curve exhibits a shift towards lower wavelengths with the decrease in the width of the QWs.

Quaternary GaAsSbN is a promising candidate for use in GaAs-based optoelectronic devices in the 1.33-1.55 μm wavelength region. We have calculated the band structure of dilute nitride-antimonide $GaAs_{1-x-y}N_xSb_y$ alloys, lattice matched to GaAs, using Band anticrossing (BAC) and Valence Band Anticrossing (VBAC) model in conjugation with the **k·p** Hamiltonian method. This mathematical model in the form of a 16 band Hamiltonian matrix is used to examine the shift of different bands as a function of Sb concentration for both bulk and quantum well structures for GaAsSbN/GaAs. The band parameters such as energy gap, spin-orbit splitting energy, carrier effective masses, band offsets, and strain generated due to the growth of GaAsSbN/GaAs heterostructures as a function of Sb and N concentrations are calculated and compared with the recent experimental data. The substitution of As atoms due to the incorporation of N and Sb impurity atoms causes a significant band gap reduction of ~330 meV for $GaAs_{0.931}Sb_{0.05}N_{0.019}$ alloys. The enhancement of spin-orbit splitting energy causes a crossover between E_g and Δ_{SO} for Sb and N concentration of 27 and 10 at % respectively. Suitable tuning of the band offset values with Sb and N concentrations makes GaAsSbN/GaAs alloy system an efficient alternative for band gap engineering and fabricating photonic device structures.

Date

ACKNOWLEDGEMENT

I take this opportunity to express my heartfelt gratitude and sincere thanks to my project supervisor **Dr. Tushar Dhabal Das**, Assistant Professor, Department of Basic And Applied Science, National Institute of Technology, Arunachal Pradesh for his constant guidance, suggestion and cordial encouragement at my very crucial stage of this dissertation work without him it could not become successful.

I am also grateful to **Dr. Dip Prakash Samajdar**, Assistant Professor, Indian Institute of Information Technology, Design and Manufacturing (IIITDM) Jabalpur for his valuable supports, suggestion and gracious encouragement whenever required, without him it could not become successful.

Finally, I want to thank my family and friends **Sahana Deb, Asish Hazra, Sabya Sachi Sahu, N. Kumar Reddy, Sirikonda Rambabu, Shivam Raj, Md. Sirajuddin Inamdar, Bharat Kaushik, Bharat Richhariya, Mirwajahat Hussain, Dileep Kumar, Sanjeet Kumar, Saikat Ghosh** for always being there for me. Their love, constant support and encouragement and motivation to pursue my goals made this thesis possible.

Indranil Mal

MCC/15/05

Place: Yupia, Papum Pare

Table of Contents

List of Figures

List of Tables

1 Introduction

Selection of suitable materials with excellent structural and optical characteristics forms the basis for the fabrication of optoelectronic devices. Bi-containing III-V alloy, GaSbBi is one of such potential candidate for the realization of numerous applications in the technologically important 2-5 μm mid-infrared window, such as spectroscopy, materials processing, chemical and biomolecular sensing, security and industry due to its important property of band gap tuning [1]. Substitution of the Sb atoms by Bi atoms in GaSb helps in reducing the band gap by the upward shift of the light hole/heavy hole band and subsequent lowering of the conduction band minimum owing to Virtual Crystal Approximation (VCA) [2]. There are a number of reports on the theoretical modeling [1-5] and experimental growth [6-9] of this bulk ternary alloy $GaSb_{1-x}Bi_x$. Band gap reduction by about 40 meV/at%Bi and enhancement of spin-orbit splitting energy by 21 meV/at%Bi is obtained using VBAC Model [1] which is consistent with the experimental results [6-9]. In addition to GaSbBi alloys, Type-II GaSb/GaAs quantum dot (QD) structures have been the subject of study by the researchers due to their applications in LEDs involving dipole transitions [10], charge storage devices [11,12] Intermediate Band solar cells [13] and quantum-dot infrared LED [14]. Type-II quantum well (QW) structures have fascinated the researchers to resolve the major challenges, like charge separation due to the existence of the built-in electric field inside the QW [15]. The primary advantage of using Type II structures in optoelectronic applications is that it helps to improve the electron-hole envelope function, which enhances the radiative efficiency of developed heterostructures [16]. A recent report on the growth and photoluminescence studies of strained Type II GaSbBi/GaAs QDs produced some interesting results [17].

Dilute III-V Nitride alloys have attracted the attention of the researchers in the past few decades due to their unique physical properties such as simultaneous reduction of band gap and lattice parameter of the corresponding III-V host lattice and potential applications in GaAs-based optoelectronic and photonic devices operating in the strategically important telecommunication wavelength range of 1.3-1.55 μm [18-21]. GaAsSbN is a favorable alternative for achieving longer wavelengths with lower N concentration compared to GaInAsN [22]. A Smaller value of energy band gap is achievable with GaAsSbN than with GaInAsN for the same nitrogen concentration as GaAsSb presents a stronger bandgap bowing than GaInAs [23]. Harmand and co-workers reported a band gap reduction of 180 meV for a nitrogen incorporation of 1% in GaAsSbN/GaAs quantum wells (QWs) [21-23]. Though GaAsSbN (QW) structures are not suitable for the fabrication of 1.3 μm GaAs-based lasers due to their weaker electron confinement compared to GaInAsN QWs, they are suitable for 1.55 μm lasers for the lesser percentage of nitrogen required to achieve the desired wavelength [21]. Higher concentration of nitrogen often leads to the formation of N-related defects which degrades the

minority-carrier lifetime and efficiency in GaInAsN based devices [24]. The presence of a single Group III element in GaAsSbN makes the nitrogen concentration insensitive to the presence of Sb unlike GaInAsN alloys where In is reported to lower the concentration of N atoms [22]. This makes the electronic band structure of GaAsSbN alloys less dependent on the alloy configuration [21]. The fact that GaAsSbN alloys can yield band gap values as low as 1 eV while maintaining lattice match with GaAs makes them ideal candidates for the fabrication of multijunction solar cells [24]. Thermal annealing in Sb-based alloys such as GaAsSbN and InGaAsSbN needed for the optimization of emission causes a larger blue-shift of the band gap compared to other dilute nitrides [25]. A recent report by Iyer *et al.* suggested that reducing the dimensionality of GaAsSbN alloy systems to nanowires can lead to the annihilation of N-induced point defects and enhanced photon collection for improving the performance of these dilute nitride nanowires in nanoscale optoelectronic devices [26]. The band gap reduction in dilute GaAsSbN alloys is explained using a double band anticrossing (BAC) model by Lin *et al.* which is a combination of BAC model for GaAsN and Valence BAC model for GaAsN [19].

Here we have calculated the band structure of GaSbBi/GaAs type-II QWs by including the effect of strain and bulk GaSbBi using14 band **k·p** Hamiltonian to estimate the band gap, spin-orbit splitting energy, effective masses, dispersion relations and band offsets with variable bismuth concentration. We have also calculated the optical gain of type-II QW structures as a function of well width and doping concentration.

We have also investigated the band structure of GaAsSbN alloys and GaAsSbN/GaAs QWs using a 16 band **k·p** Hamiltonian. We have extended the 8 band Hamiltonian for GaAs to a 16 band **k·p** model to take into account the effects of the incorporation of Sb and N related impurities more accurately. The influence of these impurities on the band parameters such as band gap and spin-orbit splitting energy, electron and hole effective masses, conduction band and valence band offsets for GaAsSbN alloys and QWs are discussed. The dissertation is organized as follows. Section 2 gives the details of theoretical models and material parameters for the calculation of electronic band structure and related band parameters of binary GaAs and GaSb, ternary GaSbBi/ GaAs QW and Quaternary GaAsSbN. The results of the 8 band,14 band and 16 band **k·p** calculations for the corresponding alloys and QWs are presented in Section 3. The effects of strain on the band structure are also discussed in this section. Section 4 summarizes the contribution of our work in the relevant field and future work.

2 Theoretical Framework

For appropriate characterization of any material, both empirical and theoretical analysis is required. For theoretical analysis, there are various kind of tool with their own better hub such as DFT, Tight Binging method, Pseudopotential method, The **k.p** method. As per the subject of interest, specific methods are being used; here we are interested in optoelectronic behavior, which primarily depends on the band edge of III-V materials. As a result, we will focus on The k.p Hamiltonian, which offers precise and reliable results near the band edge.

2.1 The k.p Hamiltonian

This numerical powerful tool helps to analyze the conduction band and valance band near the band edges of direct band-gap III-V semiconductors, where the wave vector **k** changes by a little amount from a vector $\mathbf{k_0}$ where a local maximum or minimum occurs. The **k.p** method was introduced by Bardeen [27] and Seitz [28], the method offers numerical analysis of Eigenvalue of 8×8 system Hamiltonian and provides basic 4 band electronic band structure of III-V semiconductors. The method has also been used widely by many researchers to semiconductors [29-34]. We will discuss Kane's model [31,32], which takes into account the spin-orbit interaction, and Luttinger-Kohn's models [33] for degenerate bands and further modification for Valance Band Anticrossing (VBAC) model for 14 band and 16 band respectively along with strain influence. These models are very popular in studying bulk and quantum well semiconductors and have been used during the past few decades. The Schrödinger equation for single electron

$$H\Psi(\mathbf{r}) = \left[\frac{\hbar^2}{2m_0}\nabla^2 + \nabla(\mathbf{r}) = E(\mathbf{k})\Psi(\mathbf{r})\right] \qquad 2\text{-}1$$

where $E(\mathbf{k})$ is the Eigenvalue of the electron wave function and **k** is the electron wave vector; the general solution of above equation is

$$\Psi_{n\mathbf{k}}(\mathbf{r}) = e^{i\mathbf{k}.\mathbf{r}}u_{n\mathbf{k}}(\mathbf{r}) \qquad 2\text{-}2$$

where $u_{n\mathbf{k}}(\mathbf{r})$ is the periodic Bloch function and n refers to the band. Generalize Schrödinger equation for electron with above wave function in terms of $u_{n\mathbf{k}}(\mathbf{r})$ can be written as

$$\left\{\frac{p^2}{2m_0} + \frac{\hbar}{m_0}\mathbf{k}\,.\,\mathbf{p} + V(\mathbf{r})\right\}u_{n\mathbf{k}}(\mathbf{r}) = \left[E_n(\mathbf{k}) - \frac{\hbar^2k^2}{2m_0}\right]u_{n\mathbf{k}}(\mathbf{r}) \qquad 2\text{-}3$$

This equation can be evaluated at a specific point $\mathbf{k_0}$ of interest in the Brillouin zone; at $\mathbf{k_0} = 0$, at Γ point, the above equation can be expanded as

$$\left\{H_0 + \frac{\hbar}{m_0}\mathbf{k}\,.\,\mathbf{p}\right\}u_{n\mathbf{k}}(\mathbf{r}) = \left[E_n(\mathbf{k}) - \frac{\hbar^2 k^2}{2m_0}\right]u_{n\mathbf{k}}(\mathbf{r}) \qquad 2\text{-}4$$

where

$$H_0 = \frac{p^2}{2m_0} + V(\mathbf{r}) \qquad 2\text{-}5$$

$$H_0 u_{n0}(\mathbf{r}) = E_n(0)u_{n0}(\mathbf{r}) \qquad 2\text{-}6$$

The III-V zinc-blende crystal (GaAs) formed by the contribution of outermost electron of $4s^2$ and $4p^1$ electrons with valence III (Ga) atoms and $4s^2$ and $4p^3$ electrons with valence V (As) atoms, as result the electron wave functions are p-like near the top of the valence band and S-like near the bottom of the conduction band. The first four basis functions are respectively degenerate with the last four basis functions; hence the 8x8 interaction matrix becomes [35]

$$H_{8\times8} = \begin{bmatrix}
C^8 & 0 & -\frac{1}{\sqrt{2}}P_+ & \sqrt{\frac{2}{3}}P_z & \frac{1}{\sqrt{6}}P_- & 0 & \frac{1}{\sqrt{3}}P_z & \frac{1}{\sqrt{3}}P_- \\
0 & C^8 & 0 & -\frac{1}{\sqrt{6}}P_+ & \sqrt{\frac{2}{3}}P_z & \frac{1}{\sqrt{2}}P_- & \frac{1}{\sqrt{3}}P_+ & -\frac{1}{\sqrt{3}}P_z \\
-\frac{1}{\sqrt{2}}P_+^* & 0 & H^8 & \alpha & \beta & 0 & i\frac{\alpha}{\sqrt{2}} & -i\sqrt{2}\beta \\
\sqrt{\frac{2}{3}}P_z & -\frac{1}{\sqrt{6}}P_+^* & \alpha^* & L^8 & 0 & \beta & i\left(-\frac{D^8}{\sqrt{2}}\right) & i\sqrt{\frac{3}{2}}\alpha \\
\frac{1}{\sqrt{6}}P_-^* & \sqrt{\frac{2}{3}}P_z & \beta^* & 0 & L^8 & -\alpha & -i\sqrt{\frac{3}{2}}\alpha^* & i\left(-\frac{D^8}{\sqrt{2}}\right) \\
0 & \frac{1}{\sqrt{2}}P_-^* & 0 & \beta^* & -\alpha^* & H^8 & -i\sqrt{2}\beta^* & -i\frac{\alpha^*}{\sqrt{2}} \\
\frac{1}{\sqrt{3}}P_z & \frac{1}{\sqrt{3}}P_+^* & -i\frac{\alpha^*}{\sqrt{2}} & i\left(\frac{D^8}{\sqrt{2}}\right) & i\sqrt{\frac{3}{2}}\alpha & i\sqrt{2}\beta & S^8 & 0 \\
\frac{1}{\sqrt{3}}P_-^* & -\frac{1}{\sqrt{3}}P_z & i\sqrt{2}\beta^* & -i\sqrt{\frac{3}{2}}\alpha^* & i\left(\frac{D^8}{\sqrt{2}}\right) & i\frac{\alpha}{\sqrt{2}} & 0 & S^8
\end{bmatrix} \qquad 2\text{-}7$$

where

$$C^8 = E_G + \frac{\hbar^2}{2m_0}\left[\frac{1}{m_e^*} - \frac{E_P}{3}\left(\frac{2}{E_G} + \frac{1}{E_G + \Delta}\right)\right] \times \left(k_x^2 + k_y^2 + k_z^2\right)$$

$$H^8 = -\frac{\hbar^2}{2m_0}\left[\left(k_x^2 + k_y^2\right)\left(\gamma_1 + \gamma_2\right) + k_z^2\left(\gamma_1 - 2\gamma_2\right)\right]$$

$$L^8 = -\frac{\hbar^2}{2m_0}\left[\left(k_x^2 + k_y^2\right)\left(\gamma_1 - \gamma_2\right) + k_z^2\left(\gamma_1 + 2\gamma_2\right)\right]$$

$$S^8 = -\frac{\hbar^2}{2m_0}\left[\left(k_x^2 + k_y^2 + k_z^2\right)\gamma_1\right] - \Delta$$

$$\beta = -\frac{\hbar^2}{2m_0}\sqrt{3}\left[2ik_xk_y\gamma_3 - \left(k_x^2 - k_y^2\right)\gamma_2\right]$$

$$\alpha = -\frac{\hbar^2}{2m_0}2\sqrt{3}\left[k_z\left(ik_y - k_x\right)\gamma_3\right]$$

$$P_{\pm} = P\left(k_x \pm ik_y\right), \qquad P_z = Pk_z, \qquad D^8 = L^8 - H^8 \text{ and } E_P = \frac{2m_0}{\hbar^2}P^2$$

E_G and Δ are the band gap and spin-orbit splitting of the material; Kane matrix element is denoted by P [2]. The valence band Luttinger parameters [36] (γ_1^L, γ_2^L, γ_3^L) used in 6-band Hamiltonian have to modify to use in 8-band Hamiltonian, which are called modified Luttinger parameters (γ_1, γ_2 , γ_3) and the relation between them is as follows [35-37]:

$$\gamma_1 = \gamma_1^L - \frac{1}{3}\frac{E_P}{E_G}, \quad \gamma_2 = \gamma_2^L - \frac{1}{6}\frac{E_P}{E_G}, \quad \gamma_3 = \gamma_3^L - \frac{1}{6}\frac{E_P}{E_G}$$

Evaluating the Eigenvalue of the Hamiltonian matrix, electronic band structure can be obtained along with that effective mass also can be analyzed near the band edge. Further incorporation of dilute impurity atoms will influence the host material's system Hamiltonian and degenerate the Eigenstates, which leads to Band Anticrossing Model.

2.2 Valance Band Anti Crossing Model

Incorporation of dilute impurity atoms create localized isoelectronic defect states near the extended valance band; those defect states interact with the subbands of the host material and split of the corresponding subbands into E_+ and E_- subbands, where E_+ and E_- prolong the extended nature of host material and the defect states respectively [11]. As a result effective Band gap reduces and spin-orbit splitting energy changes accordingly. Defect state will form near conduction band or valance band depend on electronegativity of the impurity atoms; high electronegative impurity atoms like **N** create defect state near conduction band and impurity atoms like Bi, Sb will create defect states near valance band of host material, which is illustrated as valance band anticrossing (VBAC) or 12 band **k.p** Hamiltonian. Incorporation of less electronegative and high volume atoms (Bi, Sb) in III-V host material (GaAs, GaSb) generate localized isoelectronic states near the valance band of the host material. The 6 (SB, Bi) related p-like impurity states perturb the basic 6×6 system Hamiltonian [2] and result in 12×12 Hamiltonian given bellow

$$H_{12\times12}=\begin{bmatrix} H_{6\times6} & V_{6\times6} \\ V_{6\times6} & E_{imp} \end{bmatrix} \qquad 2\text{-}8$$

where $H_{6\times6}=\begin{bmatrix} H^6 & \alpha & \beta & 0 & i\frac{\alpha}{\sqrt{2}} & -i\sqrt{2}\beta \\ \alpha^* & L^6 & 0 & \beta & -i\frac{D^6}{\sqrt{2}} & i\sqrt{\frac{3}{2}}\alpha \\ \beta^* & 0 & L^6 & -\alpha & -i\sqrt{\frac{3}{2}}\alpha^* & -i\frac{D^6}{\sqrt{2}} \\ 0 & \beta^* & -\alpha^* & H^6 & -i\sqrt{2}\beta^* & -i\frac{\alpha^*}{\sqrt{2}} \\ -i\frac{\alpha^*}{\sqrt{2}} & i\frac{D^6}{\sqrt{2}} & i\sqrt{\frac{3}{2}}\alpha & i\sqrt{2}\beta & S^6 & 0 \\ i\sqrt{2}\beta^* & -i\sqrt{\frac{3}{2}}\alpha^* & i\frac{D^6}{\sqrt{2}} & i\frac{\alpha}{\sqrt{2}} & 0 & S^6 \end{bmatrix}$ $\qquad 2\text{-}9$

where $L^6=-\frac{\hbar^2}{2m_0}\left[\left(k_x^2+k_y^2\right)\left(\gamma_1-\gamma_2\right)+k_z^2\left(\gamma_1+2\gamma_2\right)\right]+\Delta E_{VBM}\left(x\right)$

$$H^6=-\frac{\hbar^2}{2m_0}\left[\left(k_x^2+k_y^2\right)\left(\gamma_1+\gamma_2\right)+k_z^2\left(\gamma_1-2\gamma_2\right)\right]+\Delta E_{VBM}\left(x\right)$$

$$S^6 = -\frac{\hbar^2}{2m_0}\left[\left(k_x^2 + k_y^2 + k_z^2\right)\gamma_1\right] - \Delta - \Delta E_{SO}\left(x\right)$$

$$D^6 = L^6 - H^6$$

where x being the amount of mole fraction of impurity and $\Delta E_{VBM}\left(x\right), \Delta E_{SO}\left(x\right)$ are the valance band offset and spin-orbit offset between two basic binary material, which are also the function of impurity mole fraction.

$$V_{6\times6} = \begin{bmatrix} V^6\left(x\right) & 0 & 0 & 0 & 0 & 0 \\ 0 & V^6\left(x\right) & 0 & 0 & 0 & 0 \\ 0 & 0 & V^6\left(x\right) & 0 & 0 & 0 \\ 0 & 0 & 0 & V^6\left(x\right) & 0 & 0 \\ 0 & 0 & 0 & 0 & V^6\left(x\right) & 0 \\ 0 & 0 & 0 & 0 & 0 & V^6\left(x\right) \end{bmatrix}$$

$$E_{imp} = \begin{bmatrix} E_{imp} & 0 & 0 & 0 & 0 & 0 \\ 0 & E_{imp} & 0 & 0 & 0 & 0 \\ 0 & 0 & E_{imp} & 0 & 0 & 0 \\ 0 & 0 & 0 & E_{imp} & 0 & 0 \\ 0 & 0 & 0 & 0 & E_{imp-so} & 0 \\ 0 & 0 & 0 & 0 & 0 & E_{imp-so} \end{bmatrix}$$

Where C_{imp} is the coupling parameter and E_{imp}, E_{imp-so} is single atom energy state and spin-orbit splitting energy state of impurity atom with respect to the host atoms respectively. The Eigen value of the $H_{12\times12}$ gives the doubly degenerated valance subbands as $E^{\pm}_{HH/LH}$, $E^{\pm}_{so}$ owing to the impurity interaction with host atom's state. The E^{+} states hold the extended host atom's state and E^{-} states carry the nature of impurity atom's state. The E^{+} states lifted upward and E^{-} states dragged down with respect to the host atom's state as a result effective band gap reduction occurs [8], which is the key feature of VBAC model. Tough 12 band VBAC model remains silent about conduction band and offers detailed information about valance only but conduction band can be perturbed by conduction band offset between endpoint binary atoms and strain without incorporating another high electronegative impurity (N), which can be observed by 14 band VBAC model.

2.3 14 Band Model: $GaSb_{1-x}Bi_x$

14 band VBAC is an extension of 12 band VBAC which draws attention towards the modifications in conduction band without introducing any s-like isoelectronic defect state near conduction band edge of host atoms. Here we have considered GaSb as a host material where heavier dilute Bi replace the Sb atom and creates p-like defect states near valance band edge and splits the valance subbands of GaSb into E^+ and E^- states. Corresponding Bi impurity states and band offsets between the endpoint binary atoms GaSb and GaBi perturb the $H_{8\times8}$ and generate the 14×14 Hamiltonian given bellow

$$H_{14\times14}=\begin{bmatrix}
C^{14} & 0 & -\frac{1}{\sqrt{2}}P_+ & \sqrt{\frac{2}{3}}P_z & \frac{1}{\sqrt{6}}P_- & 0 & \frac{1}{\sqrt{3}}P_z & \frac{1}{\sqrt{3}}P_- & 0 & 0 & 0 & 0 & 0 & 0\\
0 & C^{14} & 0 & -\frac{1}{\sqrt{6}}P_+ & \sqrt{\frac{2}{3}}P_z & \frac{1}{\sqrt{2}}P_- & \frac{1}{\sqrt{3}}P_+ & -\frac{1}{\sqrt{3}}P_z & 0 & 0 & 0 & 0 & 0 & 0\\
-\frac{1}{\sqrt{2}}P_+^* & 0 & H^6 & \alpha & \beta & 0 & i\frac{\alpha}{\sqrt{2}} & -i\sqrt{2}\beta & V_{Bi}(x) & 0 & 0 & 0 & 0 & 0\\
\sqrt{\frac{2}{3}}P_z & -\frac{1}{\sqrt{6}}P_+^* & \alpha^* & L^6 & 0 & \beta & i\left(-\frac{D^6}{\sqrt{2}}\right) & i\sqrt{\frac{3}{2}}\alpha & 0 & V_{Bi}(x) & 0 & 0 & 0 & 0\\
\frac{1}{\sqrt{6}}P_-^* & \sqrt{\frac{2}{3}}P_z & \beta^* & 0 & L^6 & -\alpha & -i\sqrt{\frac{3}{2}}\alpha^* & i\left(-\frac{D^6}{\sqrt{2}}\right) & 0 & 0 & V_{Bi}(x) & 0 & 0 & 0\\
0 & \frac{1}{\sqrt{2}}P_-^* & 0 & \beta^* & -\alpha^* & H^6 & -i\sqrt{2}\beta^* & -i\frac{\alpha^*}{\sqrt{2}} & 0 & 0 & 0 & V_{Bi}(x) & 0 & 0\\
\frac{1}{\sqrt{3}}P_z & \frac{1}{\sqrt{3}}P_+^* & -i\frac{\alpha^*}{\sqrt{2}} & i\left(\frac{D^6}{\sqrt{2}}\right) & i\sqrt{\frac{3}{2}}\alpha & i\sqrt{2}\beta & S^6 & 0 & 0 & 0 & 0 & 0 & V_{Bi}(x) & 0\\
\frac{1}{\sqrt{3}}P_-^* & -\frac{1}{\sqrt{3}}P_z & i\sqrt{2}\beta^* & -i\sqrt{\frac{3}{2}}\alpha^* & i\left(\frac{D^6}{\sqrt{2}}\right) & i\frac{\alpha}{\sqrt{2}} & 0 & S^6 & 0 & 0 & 0 & 0 & 0 & V_{Bi}(x)\\
0 & 0 & V_{Bi}(x) & 0 & 0 & 0 & 0 & 0 & E_{Bi} & 0 & 0 & 0 & 0 & 0\\
0 & 0 & 0 & V_{Bi}(x) & 0 & 0 & 0 & 0 & 0 & E_{Bi} & 0 & 0 & 0 & 0\\
0 & 0 & 0 & 0 & V_{Bi}(x) & 0 & 0 & 0 & 0 & 0 & E_{Bi} & 0 & 0 & 0\\
0 & 0 & 0 & 0 & 0 & V_{Bi}(x) & 0 & 0 & 0 & 0 & 0 & E_{Bi} & 0 & 0\\
0 & 0 & 0 & 0 & 0 & 0 & V_{Bi}(x) & 0 & 0 & 0 & 0 & 0 & E_{Bi-so} & 0\\
0 & 0 & 0 & 0 & 0 & 0 & 0 & V_{Bi}(x) & 0 & 0 & 0 & 0 & 0 & E_{Bi-so}
\end{bmatrix} \qquad \text{2-10}$$

where $C^{14}=E_G+\frac{\hbar^2}{2m_0}\left[\frac{1}{m_e^*}-\frac{E_P}{3}\left(\frac{2}{E_G}+\frac{1}{E_G+\Delta}\right)\right]\times\left(k_x^2+k_y^2+k_z^2\right)+\Delta E_{CBM}\left(x\right)$

The Eigenvalues of the basic Hamiltonian at Γ point (**k**=0) gives the following set of energy states [38,39]:

$$E_{CB}=C' \qquad E_{LH/HH\pm}=\frac{1}{2}\left(H'+E_{Bi}\pm\sqrt{\left(H'-E_{Bi}\right)^2+4V_{Bi}^2}\right) \qquad \text{2-11}$$

$$E_{SO\pm} = \frac{1}{2}\left(S' + E_{Bi-SO} \pm \sqrt{\left(S' - E_{Bi-SO}\right)^2 + 4V_{Bi}^2} \right) \qquad 2\text{-}12$$

where $C' = E_g^{GaSb} + \Delta E_{CBM}(x)$, $H' = \Delta E_{VBM}(x)$ and $S' = H' - \Delta_0^{GaSb} - \Delta E_{SO}(x)$. E_g^{GaSb} is the band gap of bulk GaSb; $\Delta E_{CBM}(x)$, $\Delta E_{VBM}(x)$ and $\Delta E_{SO}(x)$ are the conduction band offset (CBO), Valance band offset (VBO) and spin-orbit split-off band offset respectively between two end point binary compounds GaSb and GaBi. The VBAC calculated band gap of the ternary alloy GaSbBi is given by the following equation: $E_g(x) = C' - \frac{1}{2}\left[\Delta E_{VBM}(x) + E_{Bi} - \sqrt{(H' - E_{Bi})^2 + 4C_{Bi}^2 x} \right]$

The 14 band **k·p** Hamiltonian is solved to calculate the dispersion relations of the different sub-bands in the three high symmetry non-equivalent crystal directions Λ, Δ and ∑ in the vicinity of Γ point. The dispersion relations are used to evaluate the effective masses of the carriers near the Brillouin zone center with the help of the following equation [40]:

$$m^* = \frac{\hbar^2}{\left| \frac{\partial^2 E}{\partial k^2} \right|_{k=0}} \qquad 2\text{-}13$$

The parameters used for the calculation of band structure and band offsets are listed in Table 1:

Table 1 List of VBAC parameters for band structure calculation

Parameters	Considered Value	Parameters	Considered Value
E_{Bi} (eV)	-1.2[5]	γ_3^L	6.0[37]
$E_{Bi\text{-}so}$ (eV)	-2.7[5]	Δ_0 (eV)	0.76[37]
C_{Bi} (eV)	1.01[5]	m_e (m_0)	0.039[37]
γ_1^L	13.4[37]	E_G (eV)	0.72[37]
γ_2^L	4.7[37]	E_P (eV)	27.0[37]

14 band model is concern about the changes in conduction band only due to endpoint binary's band offsets and strain; higher order Hamiltonian should be considered to take into account the influence of another impurity near conduction band edge.

2.4 16 Band Model : $GaAs_{1-x-y}Sb_yN_x$

The incorporation of N and Sb in GaAs causes the perturbation of the conduction and the valence bands respectively. The VBAC and Conduction Ban Anticrossing (CBAC) models take into account the effect of this perturbation using a 16 band Hamiltonian $H_{16\times16}$ obtained by the inclusion of 6 Sb-related and 2 N-related impurity states to the basic 8 band Hamiltonian of the host semiconductor matrix [38,40,41]. While the CBAC Model predicts the lowering of the Conduction Band Minimum (CBM) due to a quantum anticrossing interaction of N-related impurity states with the extended CB states of GaAs, the modification in the valence band structure due to the upward shift of the heavy hole (HH)/light hole (LH) and spin-orbit split-off (SO) bands is well-explained by the VBAC Model [2]. Electronic band structure of $GaAs_{1-x-y}N_xSb_y$ can be determined using this Hamiltonian which is the modified form of the 8 band **k·p** Hamiltonian based on the eight-band second-order Kane model applied to the zinc blende structure and Löwdin perturbation theory [35]. The resultant (16×16) matrix of the Hamiltonian can be written as [38,40]:

$$H_{16\times16} = \begin{pmatrix} H_{8\times8}^{16} & V_{8\times8}^{N,Sb}(y,x) \\ V_{8\times8}^{N,Sb}(y,x) & E_{8\times8}^{N,Sb} \end{pmatrix} \qquad 2\text{-}14$$

The matrix elements for $H_{16\times16}$ are as defined in ref. [38] for bulk GaAsNSb alloys grown on GaAs substrates. where $H_{8\times8}^{16}$ consist of $H_{8\times8}$ with slide change in diagonal elements as follows

$C^{16} = C^8 + \Delta E_{CBM}(x,y)$,

$H^{16} = H^8 + \Delta E_{VBM}(x,y)$,

$L^{16} = L^8 + \Delta E_{VBM}(x,y)$ and

$S^{16} = S^8 + \Delta E_{\mathbf{SO}}(x,y)$.

where

$$\Delta E_{CBM}(x,y) = x\Delta E_{CBM}^{GaAsN} + y\Delta E_{CBM}^{GaAsSb}$$

$$\Delta E_{VBM}(x,y) = x\Delta E_{VBM}^{GaAsN} + y\Delta E_{VBM}^{GaAsSb}$$

The 16 band Hamiltonian reduces to a 6×6 Hamiltonian at the Γ point (**k**=0) which is as given below [38]:

$$H''_{6\times6} = \begin{bmatrix} C'' & 0 & 0 & V_N(x) & 0 & 0 \\ 0 & H''/L'' & 0 & 0 & V_{Sb}(y) & 0 \\ 0 & 0 & S'' & 0 & 0 & V_{Sb}(y) \\ V_N(y) & 0 & 0 & E_N & 0 & 0 \\ 0 & V_{Sb}(x) & 0 & 0 & E_{Sb} & 0 \\ 0 & 0 & V_{Sb}(x) & 0 & 0 & E_{Sb-SO} \end{bmatrix} \quad \text{2-15}$$

where $C'' = E_g^{GaAs} + \Delta E_{CBM}(x,y)$,

$H'' = L'' = \Delta E_{VBM}(x,y)$ and

$$S'' = \frac{1}{2}(L'' + H'') - \Delta_0^{GaAs} - \Delta E_{SO}(x,y)$$

The coupling parameters $V_{Sb}(x) = C_{Sb}\sqrt{y}$ and $V_N(x) = C_N\sqrt{x}$ takes care of the coupling between the Sb impurity states and the extended valence band states and the N resonant states with the host conduction band matrix. E_N and E_{Sb} gives the energy of the N and Sb related resonant states and $E_{Sb\text{-}SO}$ is the atomic spin-orbit splitting energy for Sb. Solution of the 6 band Hamiltonian of Equation (1) yields six distinct eigen states corresponding to the splitting of the CB, HH/LH and SO bands into E^+ and E^- sub bands guided by the following equations [38]:

$$E_{HH/LH\pm} = \frac{1}{2}\left(H'' + E_{Sb} \pm \sqrt{H''^2 - 2H''E_{Sb} + E_{Sb}^2 + 4V_{Sb}(y)^2}\right) \quad \text{2-16}$$

$$E_{CB\pm} = \frac{1}{2}\left(C'' + E_N \pm \sqrt{(C''^2 - 2C''E_N + E_N^2 + 4V_N(x)^2}\right) \quad \text{2-17}$$

$$E_{SO\pm} = \frac{1}{2}\left(S'' + E_{Sb\text{-}SO} \pm \sqrt{(S''^2 - 2S''E_{Sb\text{-}SO} + E_{Sb\text{-}SO}^2 + 4V_{Sb}(y)^2}\right) \quad \text{2-18}$$

The band gap energy of the quaternary alloy $GaAs_{1-x-y}N_xSb_y$ obtained using a combination of VBAC and CBAC Models can be written as:

$$E_g(x,y)=\frac{1}{2}\left[E_g^{GaAs}+\Delta E_{CBM}(x,y)+E_N-\sqrt{(C'-E_N)^2+4C_N^2y}\right]-\frac{1}{2}\left[\Delta E_{VBM}(x,y)+E_{Sb}-\sqrt{(H'-E_{Sb})^2+4C_{Sb}^2x}\right] \quad 2\text{-}19$$

Using Vegard's law, the lattice constant of $GaAs_{1-x-y}N_xSb_y$ can be obtained as a linear interpolation of the lattice constants of the endpoint compounds [36,40].

$$a_{GaAs_{1-x-y}N_xSb_y}=(1-x-y)a_{GaAs}+ya_{GaSb}+xa_{GaN} \quad 2\text{-}20$$

The values of a_{GaAs}, a_{GaN} and a_{GaSb} as obtained from [37] are 5.653 Å, 4.50Å and 6.095Å, respectively. The above equation is used to calculate that $GaAs_{1-x-y}N_xSb_y$ can be lattice matched to GaAs substrate for a N to Sb concentration ratio x/y of 0.38. The VB and CB offsets and offset ratios are calculated employing the technique used in [38]. The parameters used for the calculation of band structure and band offsets are listed in Table 2

Table 2 List of BAC parameters for band structure calculation

Parameters	Values used in this work (eV)	Parameters	Values used in this work (eV)
E_N	0.23[19]	E_P^{GaAs}	28.8[37]
C_N	2.7 [19]	ΔE_{CBM}^{GaAsSb}	-0.06
E_{Sb}	1.0 [2]	ΔE_{VBM}^{GaAsSb}	-0.77
$E_{Sb\text{-}so}$	1.6[2]	ΔE_{SO}^{GaAsSb}	-0.35
C_{Sb}	1.05[2]	ΔE_{CBM}^{GaAsN}	0.07
E_g^{GaAs}	1.43[37]	ΔE_{VBM}^{GaAsN}	1.84
Δ_0^{GaAs}	0.341[37]	ΔE_{SO}^{GaAsN}	1.52

The above discussed VBAC and BAC model can be extended further for quantum confined structures where strain will play a crucial role , discussed latter section.

2.5 Strain Effect

The effects of strain are of particular interest in Quantum confined structures to have better optical properties. Strong lattice mismatch with the host substrate offers a large conduction and valence band offsets. Hydrostatic strain acts uniformly irrespective of carrier's effective mass of corresponding subbands nevertheless shearing strain acts in a different way to HH and LH sub band, which breaks the degeneracy of HH and LH at Γ=0, predicted by VBAC model. Hence the strain influenced perturb Hamiltonian is calculated by using the Bir-Pikus Hamiltonian [42] given bellow

$$H_{8\times8}^{Strain}=\begin{bmatrix} C & 0 & -\frac{1}{\sqrt{2}}P_+ & \sqrt{\frac{2}{3}}P_z & \frac{1}{\sqrt{6}}P_- & 0 & \frac{1}{\sqrt{3}}P_z & \frac{1}{\sqrt{3}}P_- \\ 0 & C & 0 & \frac{1}{\sqrt{6}}P_+ & \sqrt{\frac{2}{3}}P_z & \frac{1}{\sqrt{2}}P_- & \frac{1}{\sqrt{3}}P_+ & -\frac{1}{\sqrt{3}}P_z \\ -\frac{1}{\sqrt{2}}P_+^* & 0 & H & \alpha & \beta & 0 & \frac{i\alpha}{\sqrt{2}} & -i\sqrt{2}\beta \\ \sqrt{\frac{2}{3}}P_z & \frac{1}{\sqrt{6}}P_+^* & \alpha^* & L & 0 & \beta & i\left(\sqrt{2}\varepsilon-\frac{D}{\sqrt{2}}\right) & i\alpha\sqrt{\frac{3}{2}} \\ \frac{1}{\sqrt{6}}P_-^* & \sqrt{\frac{2}{3}}P_z & \beta^* & 0 & L & -\alpha & -i\alpha^*\sqrt{\frac{3}{2}} & i\left(\sqrt{2}\varepsilon-\frac{D}{\sqrt{2}}\right) \\ 0 & \frac{1}{\sqrt{2}}P_-^* & 0 & \beta^* & -\alpha^* & H & -i\sqrt{2}\beta^* & \frac{-i\alpha^*}{\sqrt{2}} \\ \frac{1}{\sqrt{3}}P_z & \frac{1}{\sqrt{3}}P_+^* & \frac{i\alpha^*}{\sqrt{2}} & i\left(\frac{D}{\sqrt{2}}-\sqrt{2}\varepsilon\right) & i\alpha\sqrt{\frac{3}{2}} & i\sqrt{2}\beta & S & 0 \\ \frac{1}{\sqrt{3}}P_-^* & -\frac{1}{\sqrt{3}}P_z & i\sqrt{2}\beta^* & -i\alpha^*\sqrt{\frac{3}{2}} & i\left(\frac{D}{\sqrt{2}}-\sqrt{2}\varepsilon\right) & \frac{i\alpha}{\sqrt{2}} & 0 & S \end{bmatrix}$$

2-21

where

$$C=\left(C^{16}or\ C^{14}\right)+\varepsilon_1(z)\ ,\qquad H=\left(H^{16}or\ H^{6}\right)+\varepsilon_2(z)\ ,$$

$$L=\left(L^{16}or\ L^{6}\right)-\varepsilon_2(z)\ ,\qquad S=\left(S^{16}or\ S^{6}\right)-\varepsilon_2(z)\ ,$$

$$P_{\pm}=P(k_x\pm ik_y)-P(e_{xx}\mathrm{k_x}\pm \mathrm{ie_{yy}k_y})\quad \text{and}\quad P_z=Pk_z\text{ - }P(e_{zz}k_z)$$

$$\varepsilon_1(\mathrm{z})=\begin{cases}2(\mathrm{a_c}+\mathrm{a_v})(1\text{-}\mathrm{c_{12}}/\mathrm{c_{11}})\mathrm{e_{xx}} & \text{in the well}\\ 0 & \text{in the barrier}\end{cases}$$

$$\varepsilon_2(z)=\begin{cases}\mathrm{b}\left(1+2\,\mathrm{c_{12}}/\mathrm{c_{11}}\right)\mathrm{e_{xx}} & \text{in the well}\\ 0 & \text{in the barrier}\end{cases}$$

where a_c and a_v are the hydrostatic deformation potential for conduction and valence band, respectively, b is the shear deformation potential, c_{11} and c_{12} are the elastic stiffness constants. $e_{xx}=a_s-a_w/a_w$ is the in plane strain where a_s and a_w are the lattice constants for the substrate and well layer, respectively. P is the Kane matrix element and is normally expressed in terms of energy units as [36,37]. All the strain corresponding parameters considered here is tabulated in Table 3

Table 3 List of strain parameters used to calculate band structure of strained QWs

Strain Parameters	GaSb	GaBi	GaAs	GaN
a (Å)	6.0959[37]	6.328 [43]	5.6532[37]	4.5[37]
a_C (eV)	-7.5[37]	-8.06 [43]	-7.17[37]	-2.2[37]
a_v (eV)	-0.8[37]	-1.16 [43]	-1.16[37]	-5.2[37]
b (eV)	-2.0[37]	-1.7 [43]	-2.0[37]	-2.2[37]
C_{11}	884.2[37]	81.6 [44]	1221[37]	293[37]
C_{12}	402.6[37]	28.1[44]	566[37]	159[37]

2.6 Optical Properties

Dilute III-V N or Bi are the promising candidate for optoelectronic devices owing to their prominent direct band gap nature along with that wide range of wavelength response. Both the inter band and inter sub band transitions offers wide range of illumination and absorption. The band offsets play crucial role in direct transitions, carrier confinement and electron hole wave function's overlap, which can be tuned by varying the impurity concentration.

2.6.1 Band Offset

Band offsets define the structures and types of QWs or QDs and enlighten on confinement of carriers and ranges of wavelength response. Band offsets can be calculated as mention above where Effective band offsets can be as follows [45]

$$\Delta E_c = |E_c(x, y) - E_c(GaAs / GaSb)| \quad 2\text{-}22$$

$$\Delta E_v = |E_v(x, y) - E_v(GaAs/ GaSb)| \quad 2\text{-}23$$

And the offsets ratios are given by:

$$Q_C = \frac{\Delta E_C}{\Delta E_g} \quad 2\text{-}24$$

$$Q_{Vs} = \frac{\Delta Ev}{\Delta E_g} \quad 2\text{-}25$$

where $\Delta E_g = \left|E_g(x, y)\right| - E_g(\text{GaAs} / \text{GaSb})$

Strain also has prominent impact on the shift of offsets as shown in the Figure2.1 and the corresponding offsets are given [46] bellow

$$\Delta E^{*}_{CB} = \Delta E_{CB}(\varepsilon = 0) + \delta E^{hy}_{CB} \quad \text{2-26}$$

$$\Delta E_{HH} = \Delta E_{VB}(\varepsilon = 0) + \delta E^{hy}_{VB} - \frac{1}{2}\delta E_{S} \quad \text{2-27}$$

$$\Delta E_{LH} = \Delta E_{VB}(\varepsilon = 0) + \delta E^{hy}_{VB} + \frac{1}{2}\delta E_{S} \quad \text{2-28}$$

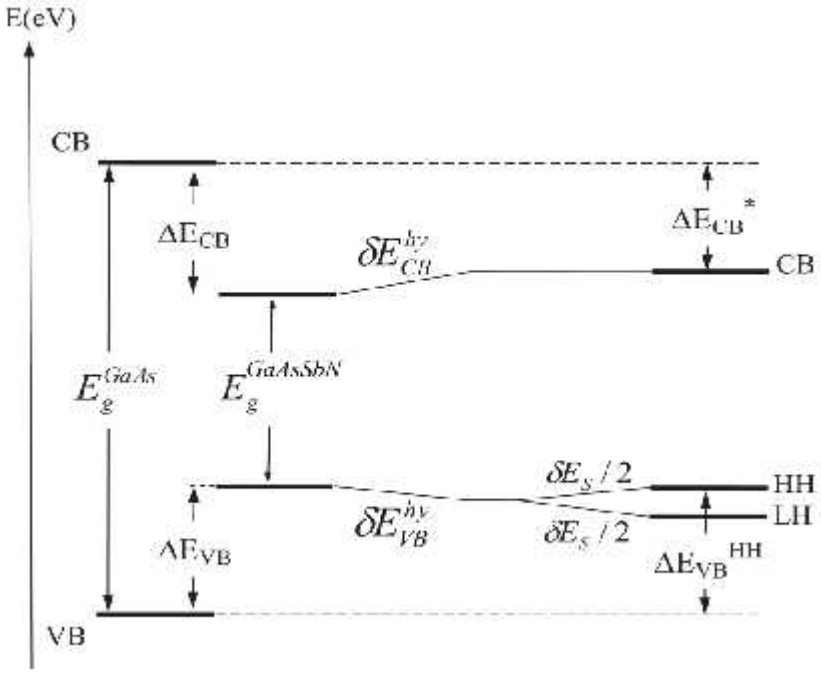

Figure2.1 Energy-space diagram of compressively strained $GaAs_{1-x-y}Sb_yN_x$ /GaAs QWs.

2.6.2 Optical Gain

The optical gain $g(\hbar\omega)$ for GaSbBi/GaAs type-II QWs is calculated by considering all the transitions between respective sub bands as per density matrix theory [47,48]. A conformist method [49] based on the intra band relaxation time (τ_{in}) approximation convoluted with a Lorentzian function with suitable broadening time ($1\times10^{-14}s$) is used to evaluate optical gain spectra[50] as follows:

$$g(\hbar\omega) = \frac{\pi q^2}{n_r c\varepsilon_0 m_0^2 \omega L_w}\sum_{n,m}\int_0^{\infty}\frac{k_p dk_p}{2\pi}\left|M_{nm}(k_p)\right|^2 L\left(E^{c,v}_{n,m}(k_p)\right)\left\{f^c_n\left(E^c_n(k_p)\right) - f^v_m\left(E^v_m(k_p)\right)\right\} \quad \text{2-29}$$

where c , ε_0 are the velocity of light and permittivity respectively in free space, n_r is the refractive index of the QW, L_w is the thickness of the QW, k_p is the in-plane

wave vector, $M_{nm}\left(k_p\right)$ is the momentum matrix element between the mth valance sub band and nth conduction band sub band . f_n^c and f_m^v are the Fermi-Dirac distribution for electrons and holes, respectively given as follows :

$$f_n^c\left(k_p\right)=\left[1+\exp\left\{\frac{E_n^c\left(k_p\right)-E_f^c}{k_BT}\right\}\right]^{-1}$$

$$f_m^v\left(k_p\right)=\left[1+\exp\left\{\frac{E_m^v\left(k_p\right)-E_f^v}{k_BT}\right\}\right]^{-1}$$

where E_n^c and E_m^v are the energy dispersion curves of the nth and the mth sub bands respectively considering the barrier effect [51], E_f^c and E_f^v are the quasi-Fermi levels of respective bands. The Lorentzian function defined in [52] is as follows

$$L\left(E_{n,m}^{c,v}\left(k_p\right)\right)=\frac{1}{\pi}\frac{\hbar/\tau_{in}}{\left[E_n^c\left(k_p\right)-E_m^v\left(k_p\right)-\hbar\omega\right]^2+\left(\hbar/\tau_{in}\right)^2}$$

3 Results and Discussion

Solution of all the above Hamiltonians offers detailed electronic band structures and effective mass of both bulk and quantum confined structures for the endpoint binary materials GaAs and GaSb with Bi, Sb and N as a impurity. 14 band model provides the detail information about electronic and optical property of ternary GaSbBi whereas 16 band model offers overall knowledge about quaternary GaAsSbN.

3.1 Electronic Properties

The Eigen values at specific point of **k** space present the band diagram near band edge, which also can provide the dispersion relation along different symmetric direction and also inform about band offsets, which are crucial parameters for optoelectronic device applications. Details information about all the host binary, ternary and quaternary is discussed bellow.

3.1.1 Binary GaAs and GaSb

Calculating the Eigen value of basic 8×8 system Hamiltonian we got the electronic band structure of GaAs and GaSb shown in Figure 3-1 and Figure 3-2

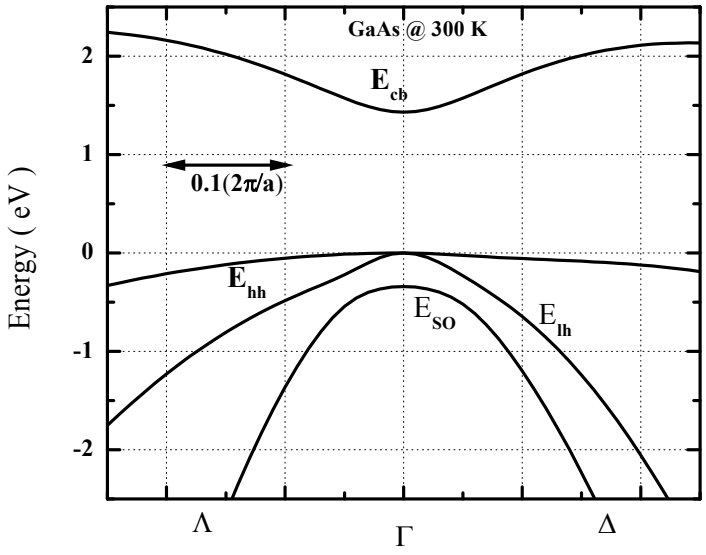

Figure 3.1 Electronic Band Diagram of GaAs

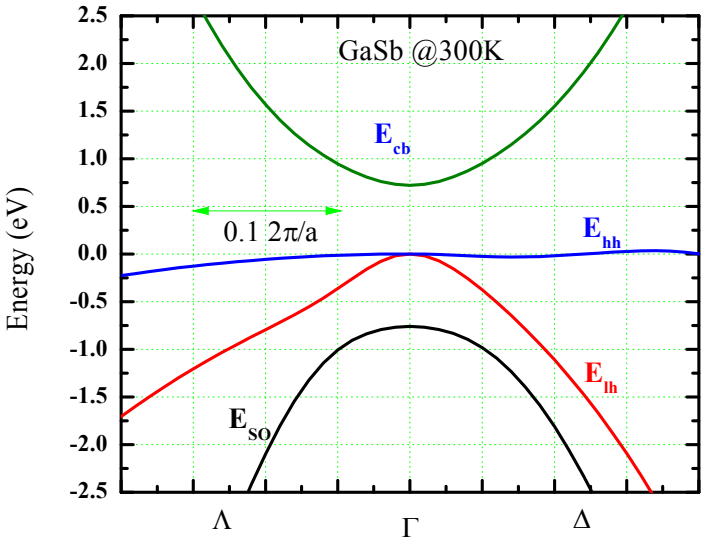

Figure 3.2 Band Diagram of GaSb Corresponding Energy states are mentioned in the diagram along different symmetric direction of crystal.

3.1.2 Ternary : GaSbBi

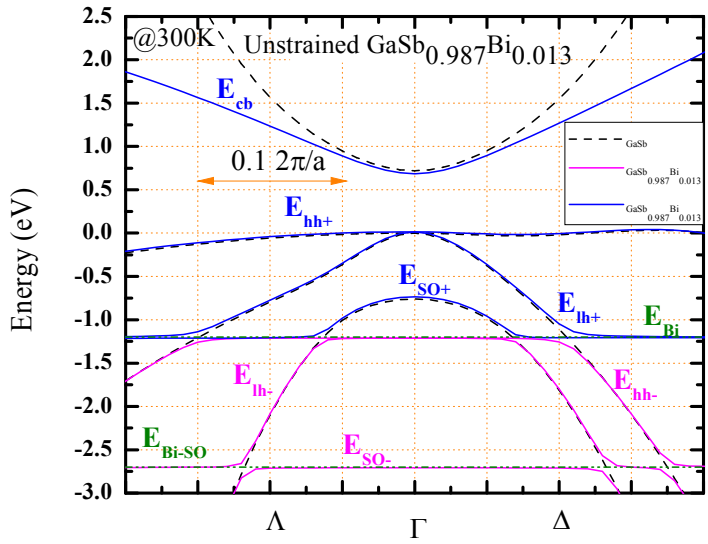

Figure 3.3 (Solid lines) Electronic band structure (BS) of unstrained $GaSb_{0.987}Bi_{0.013}$ at 300 K determined near Γ point along k-directions Δ and Λ using (14×14) VBAC model. (Dashed lines) BS of GaSb calculated using the k.p method (eight-band model). (Dash-dotted lines) EBi and EBi-SO are Bi localized levels in GaSb. Conduction band electrons, heavy holes, light holes and spin orbit splitting bands are represented by the indices cb, hh, lh and so respectively.

Solution of the 14 band Hamiltonian of Equation 2-10 yields the **E-k** diagrams shown in Figure 3.3 and Figure 3.4. Initially, we have studied the band structure of

bulk $GaSb_{0.987}Bi_{0.013}$ alloys using VBAC model [2] in which we can observe that an incorporation of 1.3% Bi in GaSb pushes the conduction band minima downward by 36 meV and shifts the valance band maxima upward by 15 meV which implies a band gap reduction of 51 meV (~39 meV/%Bi). The spin-orbit split-off band also exhibits an upward movement of 10.3 meV. Our calculated value of band gap reduction agree well with experimental results [3,4,7-9]. However, the generation of strain due to the growth of GaSbBi/GaAs QWs affects the BS significantly. The splitting of the LH and HH bands and the upward shift of the CB results in a huge band gap of 1.12 eV. The separation of the LH and HH bands by about 373 meV is comparable to that of 400 meV [17] calculated using macroscopic theory of elasticity [53]. The spin-orbit split-off band E_{SO+} also moves downward by 230 meV which increases the spin-orbit splitting energy appreciably.

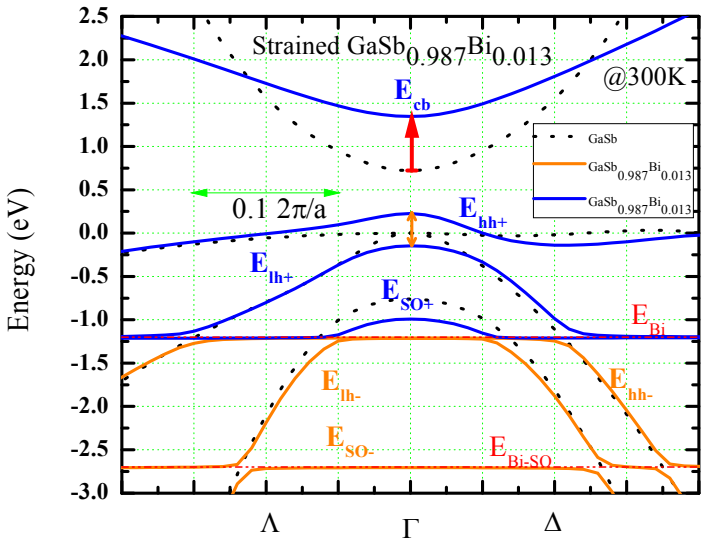

Figure 3.4 (Solid lines) Electronic band structure (BS) of strained $GaSb_{0.987}Bi_{0.013}$ at 300 K determined near Γ point along k-directions Δ and Λ using (14×14) VBAC model. (Dashed lines) BS of GaSb calculated using the k.p method (eight-band model). (Dash-dotted lines) E_{Bi} and $E_{Bi\text{-}SO}$ are Bi localized levels in GaSb. Conduction band electrons, heavy holes, light holes and spin orbit splitting bands are represented by the indices cb, hh, lh and so respectively.

Higher value of Δ_{SO} than E_g observed in GaSbBi [5] suppresses the Auger recombination loss mechanisms in optoelectronic devices such as LASERs and photodetectors thereby enhancing their efficiency and also reducing the spin lifetime of the conduction electrons. Therefore, GaSbBi system may find potential applications in the area of Spintronics [54-56].

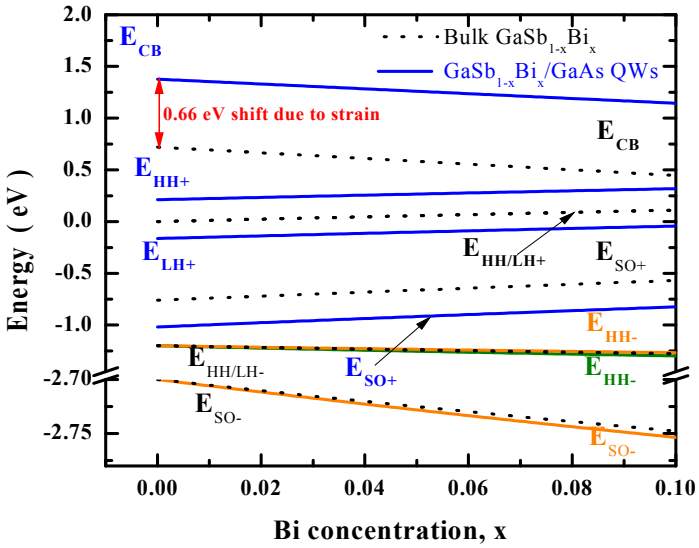

Figure 3.5 Variation of the E_+ and E_- sub band energy levels as a function of Sb concentration showing a decrease in band gap energy E_G due to the downward movement of E_{CB-} and upward movement of $E_{HH/LH+}$; solid lines represent energy level for QW structure and the dashed for bulk $GaSb_{0.987}Bi_{0.013}$.

The carrier confinement and strain immensely affects the CB and causes an upward shift of CB by 0.66 eV with respect to the host CB. As can be observed from Figure 3.5, CB and E_+ energy levels corresponding to the LH, HH and SO sub bands for GaSbBi/GaAs QWs show large deviation from their respective values for bulk GaSbBi alloys. However, the E_- sub bands are the least affected.

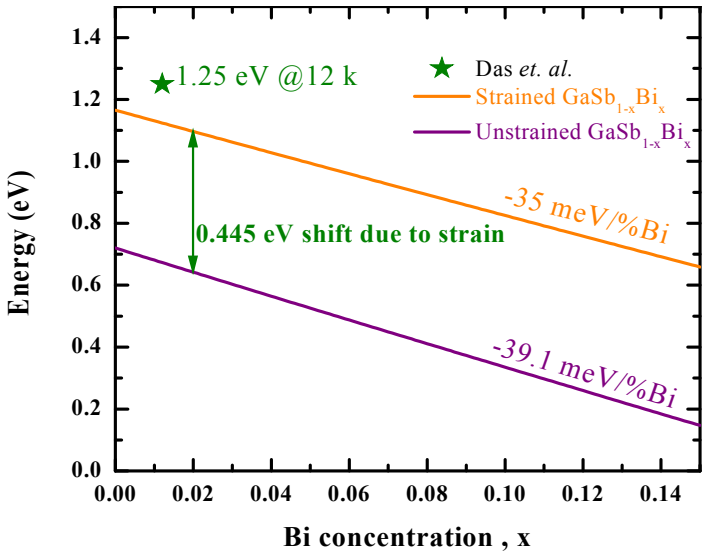

Figure 3.6 Comparison of the calculated and experimental values of band gap E_g as a function of Sb mole fraction for both the bulk and QW structure. the parenthesis reflect the slope of the curves.

For GaSbBi/GaAs QWs, the slopes of the CB, HH, LH and SO E_+ bands are -23.4 meV/%Bi, 21.3 meV/%Bi, 12.8 meV/%Bi and 11.2 meV/%Bi respectively and are calculated by solving the equations 2.11 and 2.12. Figure 3.6 clearly shows that the combined effect of strain and confinement potential increases the band gap for GaSbBi/GaAs QWs in comparison to GaSbBi alloys. However, introduction of Bi impurities in GaSb reduces the band gap by 35 meV/%Bi and 39.1 meV/%Bi respectively for QWs and bulk.

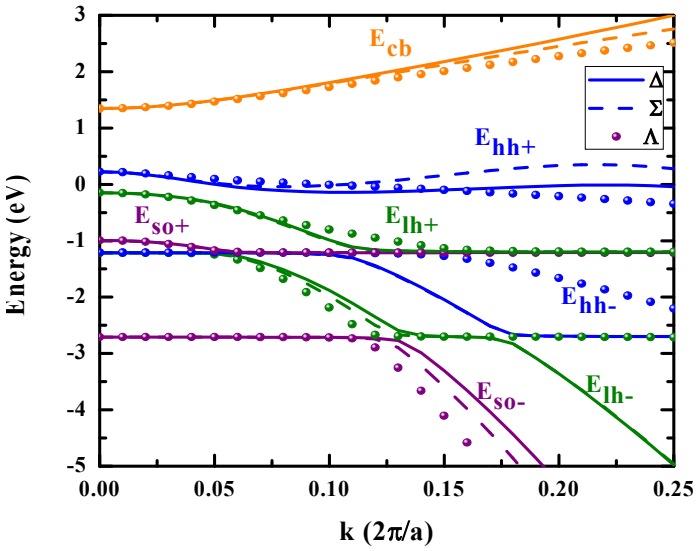

Figure 3.7 Dispersion relations for different energy levels as a function k of $GaSb_{0.987}Bi_{0.013}$ along different high symmetric directions.

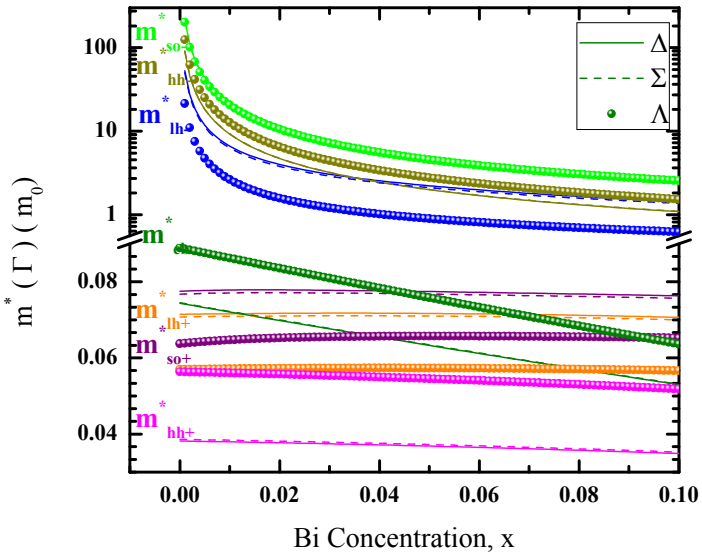

Figure 3.8 Variation of effective masses with respect to Bi mole fraction at Γ point of $GaSb_{0.987}Bi_{0.013}$ along.

It can also be observed that for a Bi incorporation of 13.2 at%, the band gap for QWs is equivalent to the band gap of GaSb alloys. A recent report by Das *et al.* on GaSbBi/GaAs Quantum dots demonstrated a band gap of 1.25 eV for a Bi incorporation of 1.2 at%Bi using photoluminescence measurements [17]. The value of the band gap of 1.17 eV calculated theoretically in this report exactly matches our calculated value of band gap for GaSbBi/GaAs QWs. We have calculated the dispersion relation $E_{u\pm}(\mathbf{k})$ for the different sub bands along the three high symmetry **k-** directions (Δ, Λ and Σ) at Γ point using the k·p Hamiltonian to observe the effect of inclusion of Bi on effective masses $m_u^*(\Gamma)$ of carriers in $GaSb_{0.987}Bi_{0.013}$/GaAs QWs where u = cb, hh, lh and so. Figure 3.7 depicts the calculated variation of the different energy levels as a function of k where it can be observed that only the variation of E_{so+} is isotropic in all orientation of **k** upto k=0.10 $Å^{-1}$. On the other hand, E_{cb-} and E_{so-} reflects a moderate change with **k**-direction beyond the value of k=0.12 $Å^{-1}$. $E_{hh/lh\pm}$ bands maintain their **p**-like nature and vary appreciably with the high symmetry **k** directions.

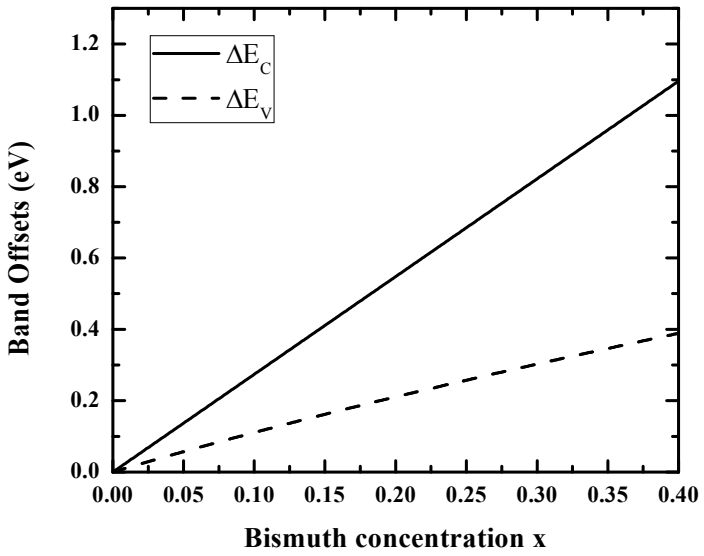

Figure 3.9 Variation of conduction and valance band offsets of GaSbBi with respect to Bismuth mole fraction

The effective masses of charge carriers belonging to different sub bands calculated using Equation (2.13) in the vicinity of the Brillouin zone center is very significant for optical gain calculation. The variation of effective masses $m_u^*(\Gamma)$ with respect to the variation of Bi concentration @300K along the three high symmetry unlike **k-** directions (Δ, Λ and Σ) are shown in Figure 3-8. The effective mass of electron m_e^* obtained from the value of m_{cb}^* = 0.09 m_0 is higher than the value 0.039 m_0 for GaSb [37] which is due to the confinement of electrons in the QW structure. The carrier effective masses m_{hh+}^*, m_{lh+}^* and m_{so+}^* in the upper sub bands

are almost isotropic. The spin-orbit split-off band effective mass m^*_{so+} of 0.063 m_0 is almost five times higher than that of GaSb (0.012 m_0).

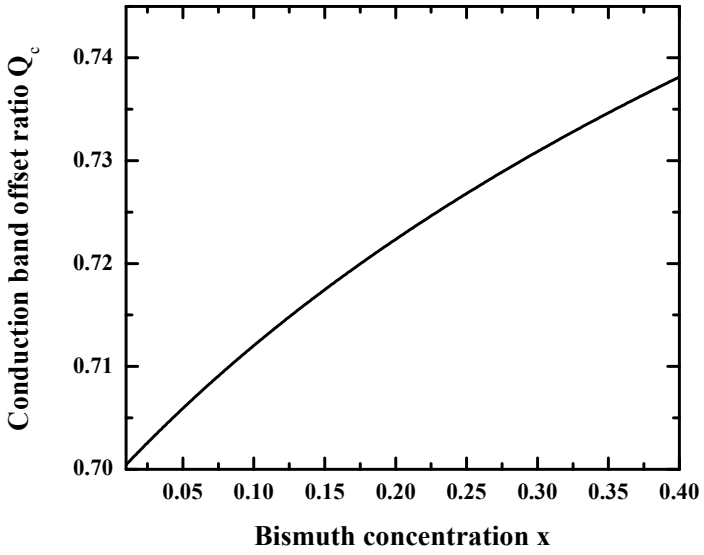

Figure 3.10 Conduction band offset ratio of GaSbBi with respect to Bismuth mole fraction

Figure 3.9 shows the variation of conduction band offset (CBO) and valance band offset (VBO) with respect to the bismuth mole fraction. It can be observed that CBO is almost 3times greater than VBO and both the VBO and CBO increase with the increase in Bi concentration.

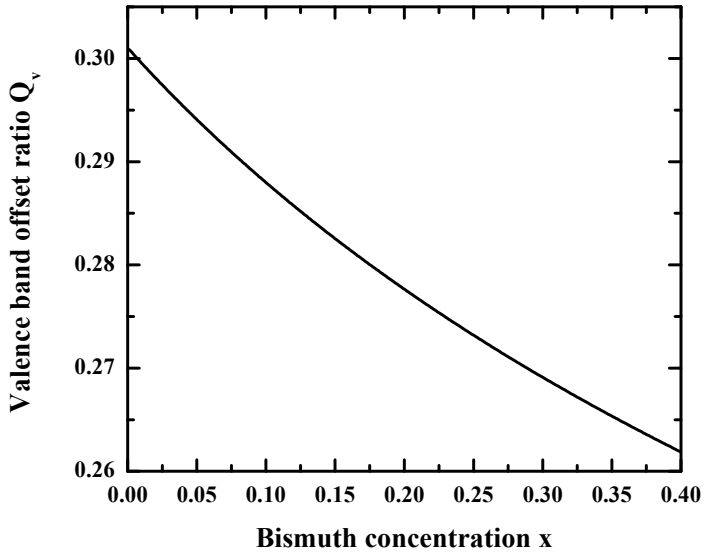

Figure 3.11 Conduction band offset ratio of GaSbBi vs Bi mole fraction

The larger value of CBO is beneficial in the sense that the optoelectronic devices fabricated using GaSbBi could provide better electron confinement.

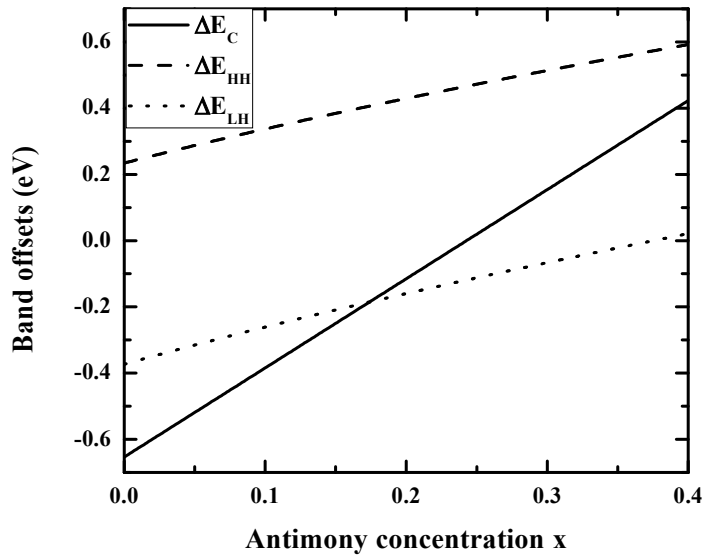

Figure 3.12 Predicted band offsets of the conduction band (ΔE_{cb}), heavy-hole (ΔE_{hh}) and light-hole (ΔE_{lh}) valence bands for GaSbBi/GaAs as a function of Bi mole fraction at 300K.

Unlike the linear increase in VBO and CBO, the VBO and CBO ratio changes non-linearly with Bi mole fraction shown in Figure 3-10 and Figure 3-11. The offset ratios can be defined as the ratio between the change in offset values to the change in band gap as a result of the incorporation of Bi impurity atoms. It can be observed from the figures that the CBO and VBO ratios exhibit opposite nature, i.e. while CBO ratio increases with Bi concentration, VBO decreases. Considering strain effect CBO and VBO have been calculated shown in Figure 3-12. It can be observed that shearing strain breaks the degeneracy of heavy hole and light hole offset.

3.1.3 Quaternary : GaAsSbN

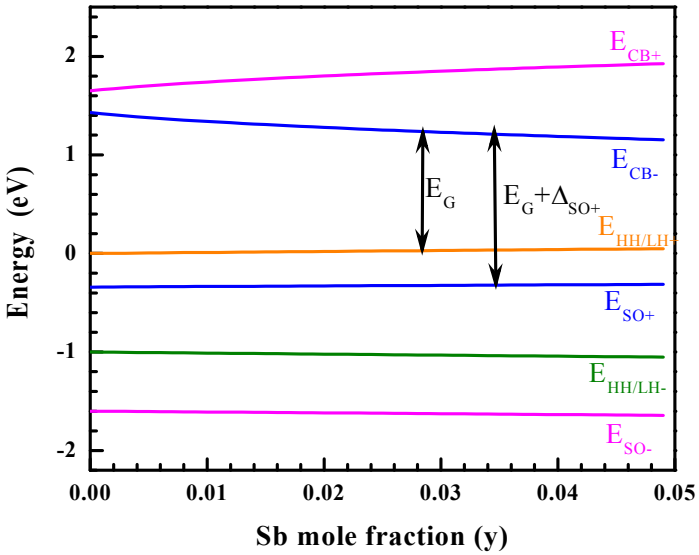

Figure 3.13 Variation of the E_+ and E_- energy levels corresponding to the CB, HH, LH and SO bands as a function of Sb concentration showing a decrease in band gap energy E_G due to the downward movement of E_{CB-} and upward movement of $E_{HH/LH+}$

Figure 3.13 shows the relative energy positions of the CB, HH/LH and SO sub bands as a function of Sb mole fraction under lattice-matched condition at the Γ point. The above figure is obtained by solving the 6 band Hamiltonian in Equation (2.15) that yields 6 distinct Eigen values corresponding to Equations 2.16-18. The anticrossing interactions of the CB, HH/LH and SO sub bands with the N and Sb related impurity states causes the repulsive movement of the E_+ and E_- energy levels. The incorporation of N and Sb in GaAs pushes the energy levels E_{CB-} in the downward direction by about 90 meV/%Sb and $E_{HH/LH+}$ in the upward direction by 10.3 meV/%Sb thereby causing a band gap reduction of ~100 meV/%Sb. The contribution of the lowering of the conduction band minimum to the total band gap reduction is about 90% which is due to the large value of the coupling parameter C_N. The spin-orbit split-off energy level E_{SO+} moves upward by 6 meV per y=0.01 which indicates that there is a slight increase of the spin-orbit splitting energy. Figure 3.14 shows the band structure of $GaAs_{0.931}N_{0.019}Sb_{0.05}$ in the Δ and Λ directions near the Γ point at room temperature. As can be observed from this E-k diagram, the impurity levels E_N, E_{Sb} and $E_{Sb\text{-}SO}$ interacts with CB, HH, LH and SO bands of the host semiconductor to split them into their corresponding spin-degenerate E_+ and E_- sub bands in accordance with Pauli's exclusion principle. The lowering of the CBM (shown by an arrow) and the slight upward movement of the HH/LH band is the primary factor responsible for band gap reduction in this quaternary alloy.

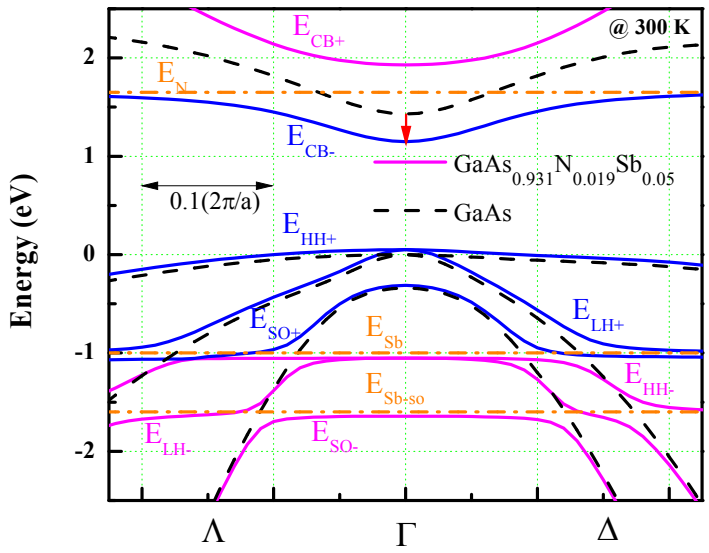

Figure 3.14 Band structure of $GaAs_{0.931}N_{0.019}Sb_{0.05}$ (solid lines) and host GaAs (dotted lines) in the crystal directions Δ and Λ at room temperature. The downward movement of the E_{CB-} energy band is indicated by an arrow (red).

For comparison the band structure of GaAs (dotted lines) is included in the same figure. A marked decrease in the CBM by an amount 281 meV and a comparatively lower increase in the VBM by about 49 meV leads to a band gap reduction of 330 meV.

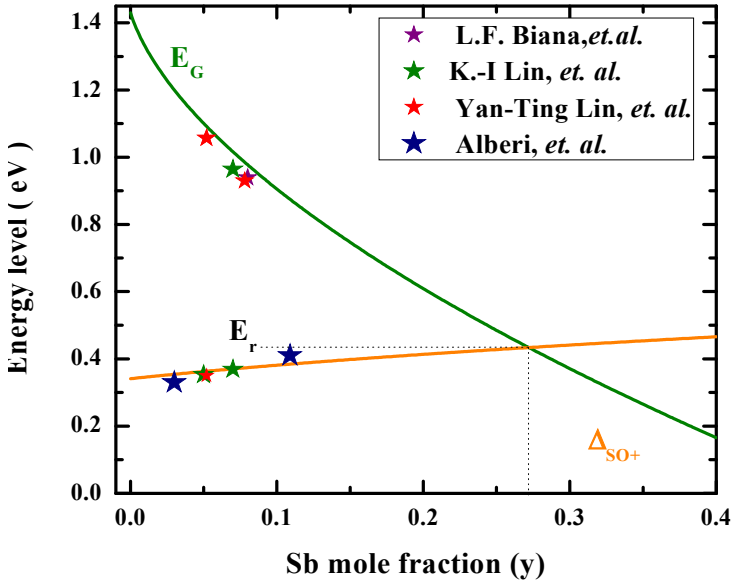

Figure 3.15 Comparison of the calculated and experimental values of band gap E_g and spin-orbit splitting energy as a function of Sb mole fraction. The resonant energy E_r is 0.44 eV for Sb concentration of 2.7 at%.

The comparison of band gap energy for $GaAs_{0.931}N_{0.019}Sb_{0.05}$ (1.10 eV) with that of $GaAs_{0.977}N_{0.023}$ (1.11 eV) [40] shows that the introduction of Sb impurity atoms in GaAs reduces the N content form 2.3 at% to 1.9 at%. This reduction in nitrogen composition improves the structural and optical properties of GaAsNSb. The E_{CB}- energy level moves downward by 0.256 eV and the increase in the VBM by 0.032 eV leads to a large band gap reduction of 0.288 eV. The spin-orbit splitting energy

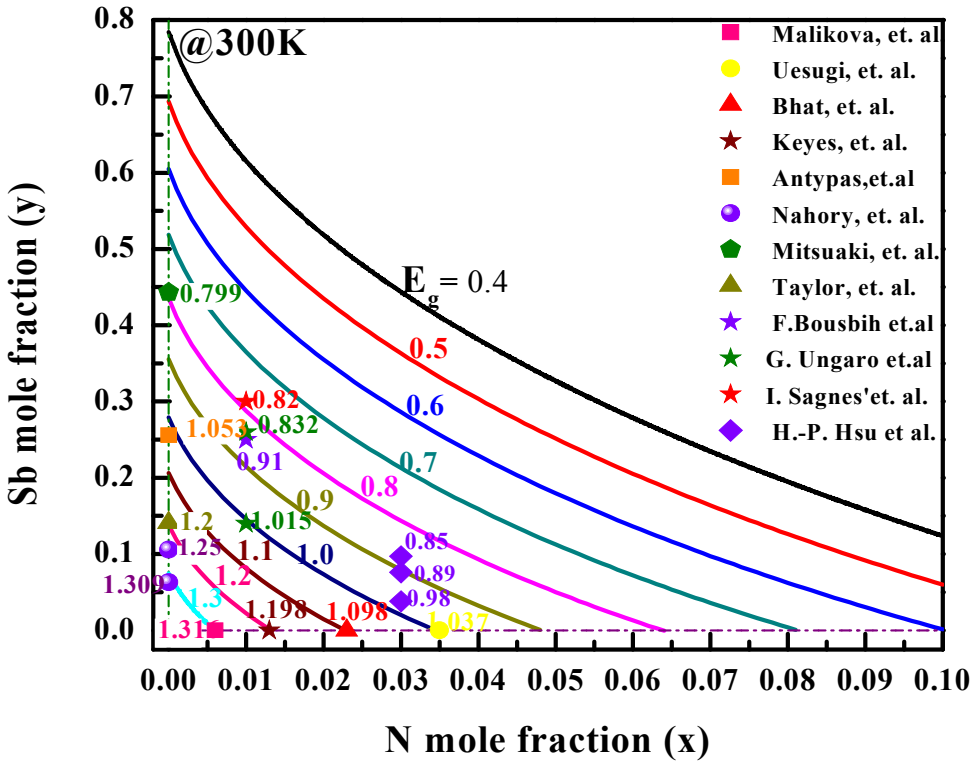

Figure 3.16 E_g for $GaAs_{1-x-y}N_xSb_y$ in the range 0.4-1.3 eV with increment of 0.1 eV as a function of both Sb and N mole fraction. Experimental values of band gap are added from the literature and good agreement exists between our calculated results and experimental values.

Δ_{SO+} increases by ~22 meV. This enhancement of spin-orbit splitting energy for GaAsNSb is much smaller in comparison to that of GaAsNBi (56 meV/%Bi) [40]. We have represented a crossover between band gap energy E_g and spin-orbit splitting energy Δ_{SO+} in

Figure 3.15. This crossover obtained for Sb = 27% and N = 10% results in the formation of $E_g<\Delta_{SO}$ regime which is known to suppress the Auger recombination processes in optoelectronic devices. Our calculations show excellent agreement with the experimental values of E_g and Δ_{SO} illustrated in the literature [19,57]. Figure 3-16 shows the variation of energy band gap for GaAsNSb alloys as a function of both Sb and N concentration at room temperature. It can be observed from the graph that VBAC calculated values of the band gap agrees well with the experimental data [22,58-68]. Band gap values in the range 0.4 eV-1.3 eV can be obtained by varying the Sb and N mole fractions. GaAsNSb can be used as 1 eV

band gap material for solar cell applications by using either an Sb concentration of 3.5 at% or N concentration of 2.5 at%.

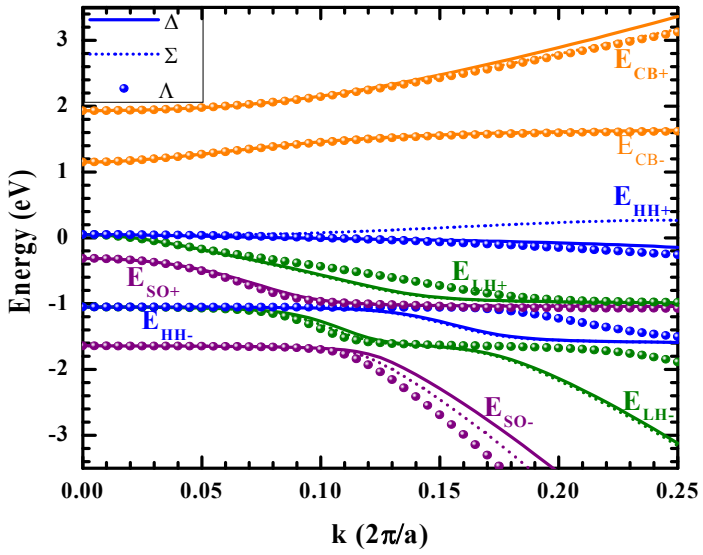

Figure 3.17 Dispersion relations $E_{\pm}$ (k) for CB, HH, LH and SO bands in the crystal directions Δ, Σ and Λ

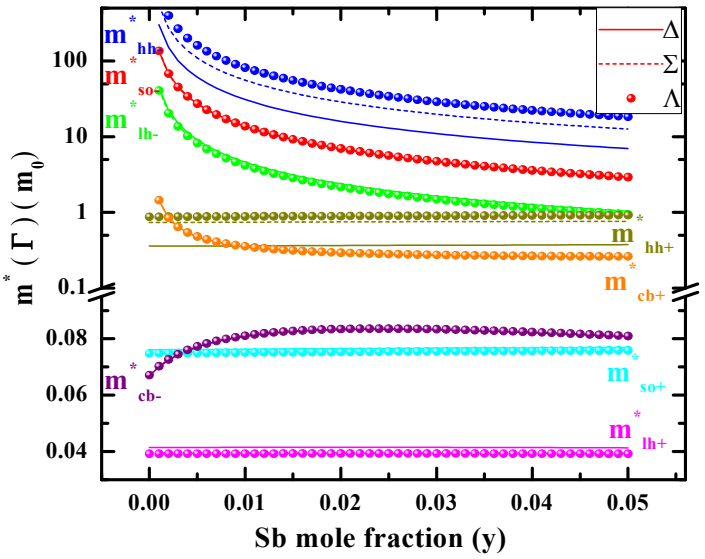

Figure 3.18 Changes in the effective masses $m^*(\Gamma)$ in the crystal directions Δ, Σ and Λ in the lower and upper valence and conduction sub bands with the variation of Sb mole fraction in the range 0-0.05.

In order to calculate the effective masses of carriers, the dispersion relation $E_{\pm}$ (k) for $GaAs_{0.931}N_{0.019}Sb_{0.05}$ lattice matched to GaAs are calculated in the high symmetry crystal directions (Δ, Σ and Λ). From Figure 3.17, we can observe that out of all the eight sub bands, only E_{CB-} and E_{SO+} are isotropic with **k** vector orientation. The bands $E_{HH\pm}$ and $E_{LH\pm}$ are highly anisotropic due to their p-like symmetry [40]. The variation of the effective masses $m^*(\Gamma)$ as a function of Sb

mole fraction in the three crystal directions Δ, Σ and Λ for T=300K is shown in Figure 3.18.

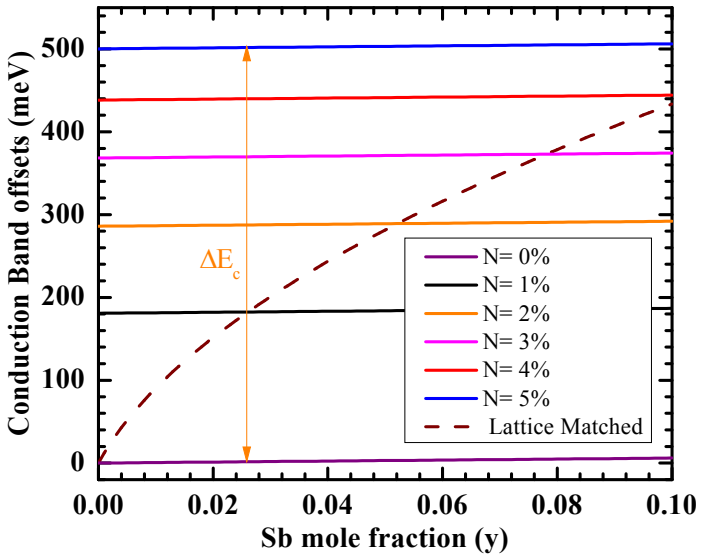

Figure 3.19 Variation of CBO for GaAsNSb versus Sb mole fraction (y) for different values of N concentration in the material. Dashed lines are used to represent the lattice matched condition (x/y =0.38).

greater than the free electron mass m_0 for the entire studied range. Hence, we are interested only with the effective masses m^*_{hh+}, m^*_{lh+}, m^*_{SO+} and m^*_{cb-} which can contribute to the transport phenomenon of in GaAsNSb. While the HH/LH effective masses show anisotropy with changes in k, effective masses of the carriers in the SO and CB bands are isotropic and exhibit s-like symmetry.

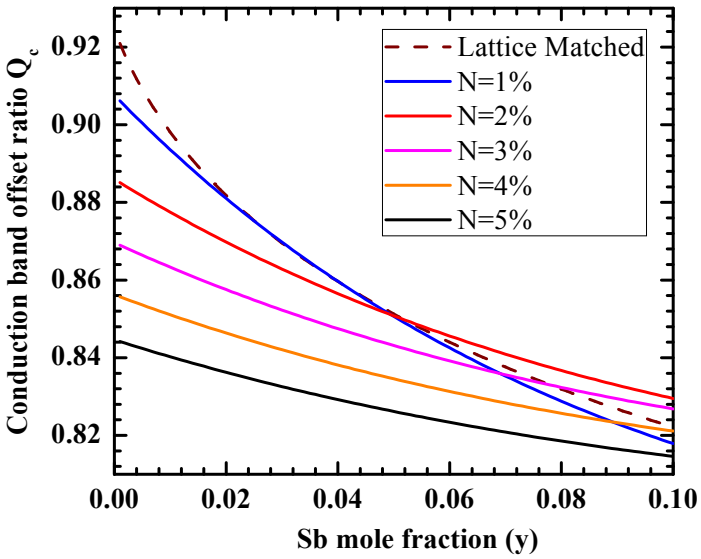

Figure 3.20 Variation of CBO ratio for GaAsNSb versus Sb mole fraction (y) for different values of N concentration in the material. Dashed lines are used to

represent the lattice matched condition (x/y =0.38).

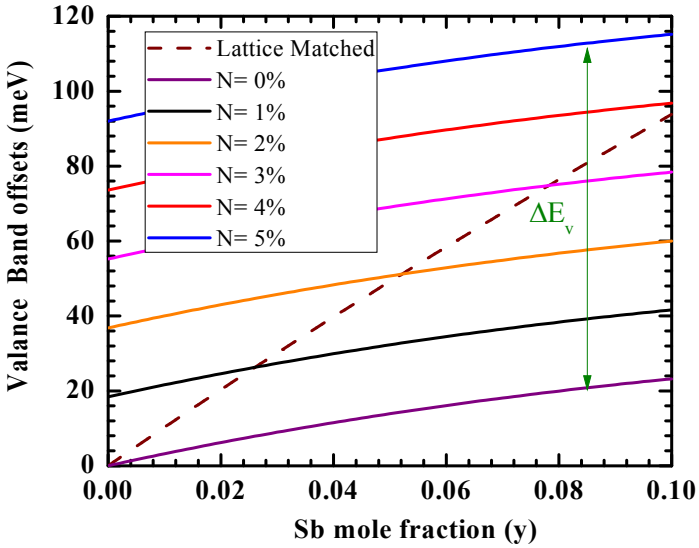

Figure 3.21 Variation of VBO for GaAsNSb versus Sb mole fraction (y) for different values of N concentration in the material. Dashed lines are used to represent the lattice matched condition (x/y =0.38).

Unlike the effective masses m^*_{hh-}, m^*_{lh-}, m^*_{SO-} and m^*_{cb+} which decreases with the increase in Sb concentration, m^*_{hh+}, m^*_{lh+} and m^*_{SO+} show just the opposite trend. m^*_{cb-} first shows an increase in value but decreases beyond y=3%. Since the carrier mobility is proportional to the inverse of the carrier effective mass, it can be inferred that unlike the dilute nitrides, the electron mobility in GaAsNSb increases

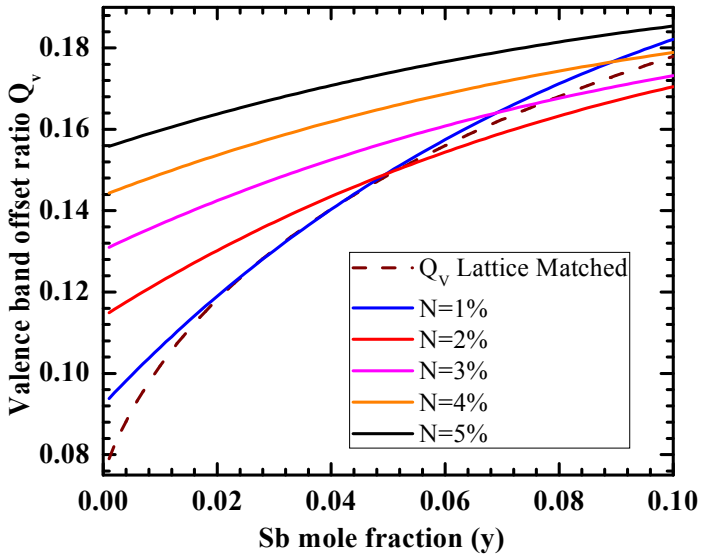

Figure 3.22 Variation of CBO ratio for GaAsNSb versus Sb mole fraction (y) for different values of N concentration in the material. Dashed lines are used to

represent the lattice matched condition (x/y =0.38).

for y>3% and the hole mobility decreases with the increase in Sb concentration as reported by Kini *et al* [69]. The value of the electron effective mass for GaAs (calculated using the 8 band k·p model) of $0.067m_0$ is exactly the same as in ref. [37]. However, the spin-orbit split-off hole effective mass shows a higher value of $0.76m_0$. Figure 3.19, Figure 3.20, Figure 3.21 and Figure 3.22 show the variation of VB offset (VBO) and CB offset (CBO) and corresponding offset ratios as a function of Sb mole fraction under lattice matched condition.

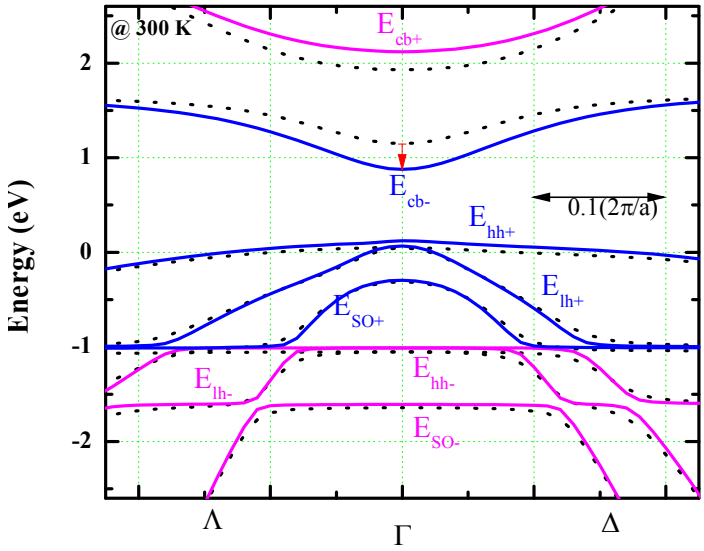

Figure 3.23 Band structure of tensile strained GaAsNSb/GaAs QWs near the Γ point in the k directions (Δ and Λ). Dashed lines indicate the band structure of GaAsNSb alloy lattice matched to GaAs substrate.

It can be observed form figures 6 (a) and (c) that the CBO is almost five times the VBO and both the VBO and CBO increase with the increase in Sb and N concentration.

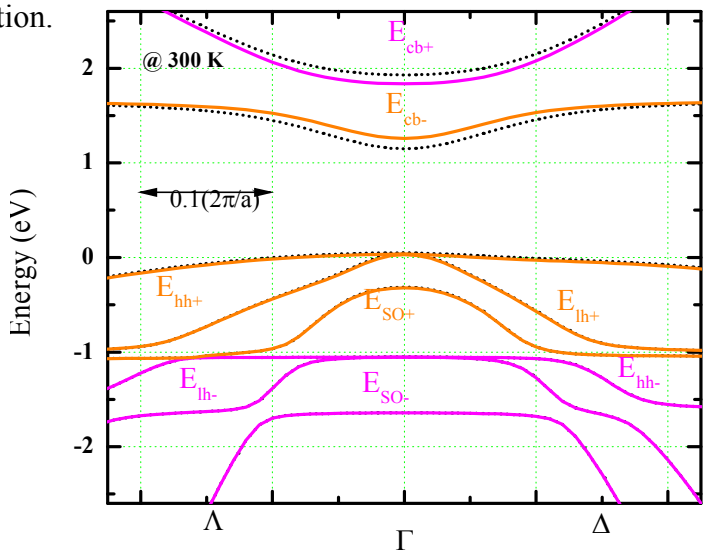

Figure 3.24 Band structure of compressive strained GaAsNSb/GaAs QWs near the Γ point in the k directions (Δ and Λ). Dashed lines indicate the band structure

of GaAsNSb alloy lattice matched to GaAs substrate.

The larger value of CBO is beneficial in the sense that the optoelectronic devices fabricated using GaAsNSb could provide better electron confinement. Unlike the linear increase in VBO and CBO, the VBO and CBO ratio changes non-linearly with Sb and N mole fraction. The offset ratios can be defined as the ratio between the change in offset values to the change in band gap as a result of the incorporation of Sb and N impurity atoms. It can be observed from the figures that the CBO and VBO ratios exhibit opposite nature, i.e. while CBO ratio decreases with Sb and N concentration, VBO increases.

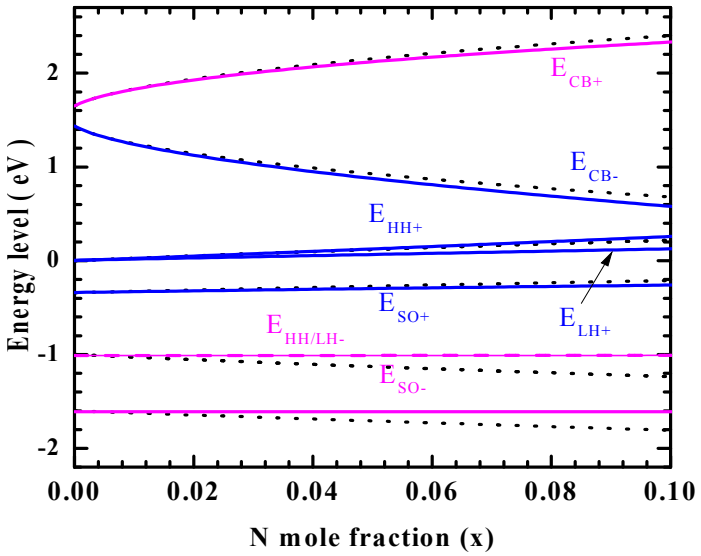

Figure 3.25 Relative positions of the energy levels $E_{\pm}$ corresponding to the CB, HH, LH and SO bands as a function Sb mole fraction for tensile strained GAAsNSb/GaAs QWs. Dashed lines represent the lattice matched condition.

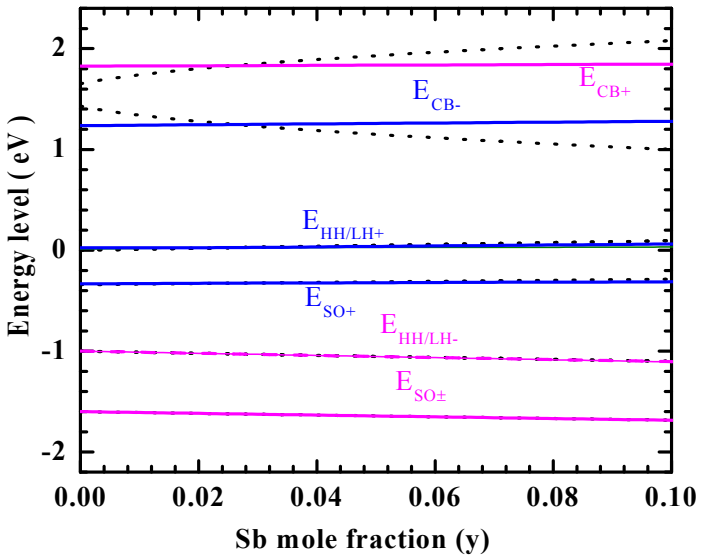

Figure 3.26 Relative positions of the energy levels $E_{\pm}$ corresponding to the CB, HH, LH and SO bands as a function of Sb mole fraction for compressive strained GAAsNSb/GaAs QWs. Dashed lines represent the lattice matched condition.

Figure 3.23 and Figure 3.24 are used to depict the difference in band structure of tensile strained and compressive strained GaAsSbN/GaAs QW structures. Tensile strain and compressive strain is plotted for N to Sb concentration ratio of 5 and 0.2 respectively which is greater or less than the lattice matched N to Sb concentration ratio of 0.38.

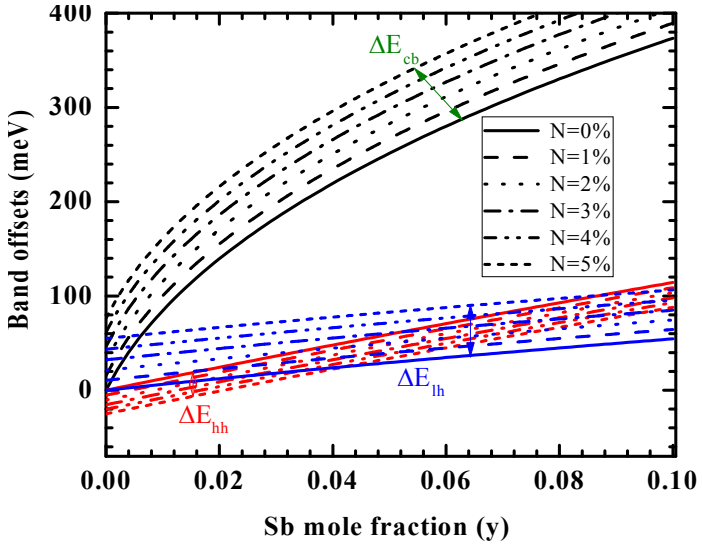

Figure 3.27 Predicted band offsets of the conduction band (ΔE_{cb}), heavy-hole (ΔE_{hh}) and light-hole (ΔE_{lh}) valence bands for GaAsNSb/GaAs as a function of Sb mole fraction at different N composition at 300K.

Splitting of LH and HH E_+ bands and bandgap as low as 0.75 eV is is observed for tensile strained $GaAs_{0.94}N_{0.05}Sb_{0.01}$/GaAs QW unlike compressive strained $GaAs_{0.94}N_{0.01}Sb_{0.05}$/GaAs QW where such appreciable splitting is not observed and a higher value of band gap of 1.22 eV is obtained.

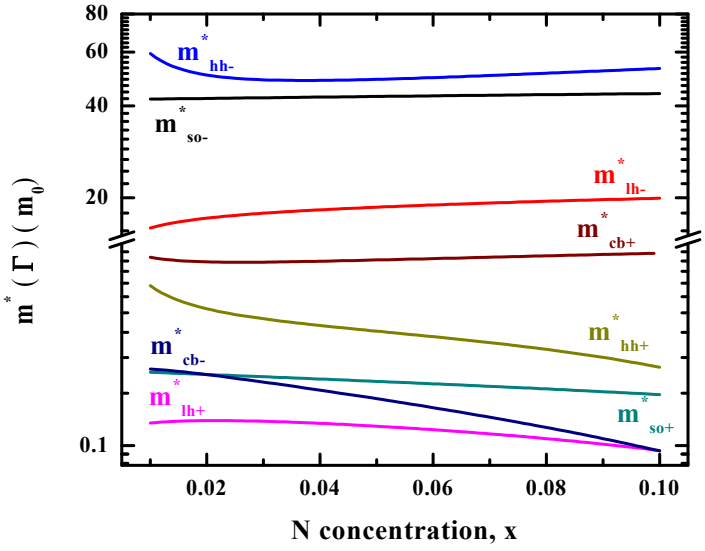

Figure 3.28 Effective masses $m^*(\Gamma)$ of the electrons and holes in the upper and lower conduction and valence sub bands versus N concentration in the crystal direction Δ.

Generation of tensile strain results in large separation between CB E_+ and E_- energy levels indicating the effect of large concentration of N atoms on the CB of GaAsSbN /GaAs QWs. Figure 3.25 **and**

Figure 3.26show the variation of CB and VB related E_+ and E_- energy levels for strained GaAsNSb/GaAs QWs.

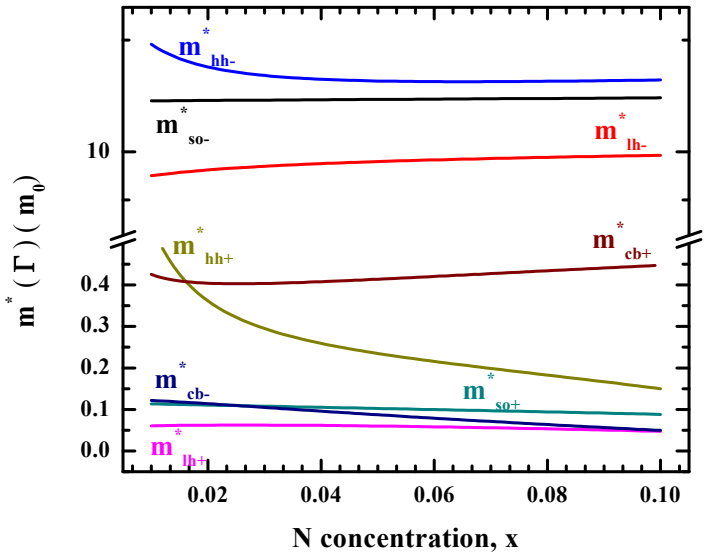

Figure 3.29 Effective masses $m^*(\Gamma)$ of the electrons and holes in the upper and lower conduction and valence sub bands versus N concentration in the crystal direction Σ.

Clearly, the figures indicate that the deviation of the energy levels from the lattice-matched condition (shown by dotted lines) is more appreciable in tensile strained QWs.

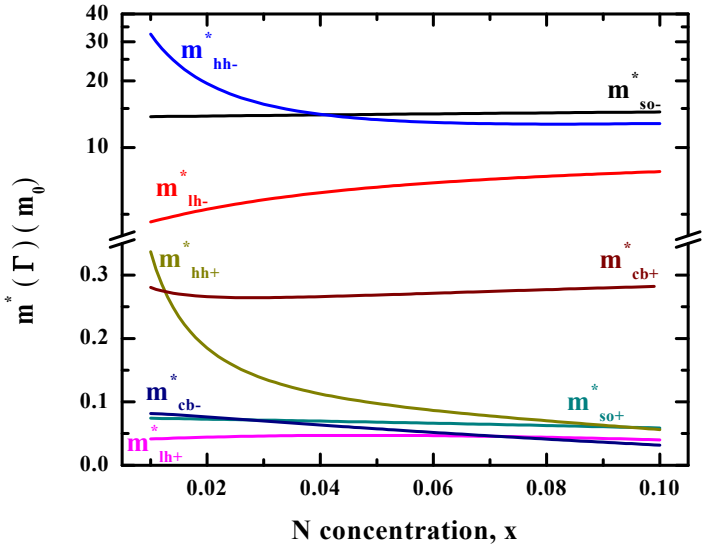

Figure 3.30 Effective masses $m^*(\Gamma)$ of the electrons and holes in the upper and lower conduction and valence sub bands versus N concentration in the crystal direction Λ.

This may be indicative of the fact that the effect of N atoms on the band structure is more than the Sb impurity atoms. Unlike the non-linear variation of E_{CB+} and

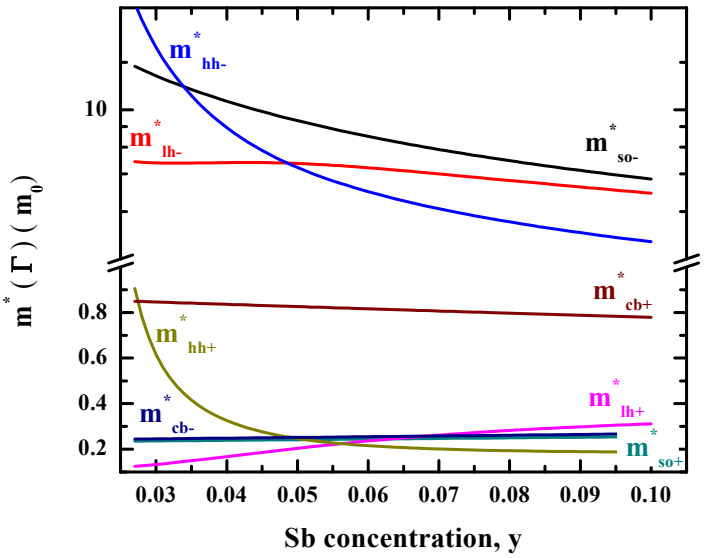

Figure 3.31 Effective masses $m^*(\Gamma)$ of the electrons and holes in the upper and lower conduction and valence sub bands versus Sb concentration in the crystal direction Δ.

E_{CB-} in with the increase in N concentration level in tensile strained structures, the energy levels vary linearly in case of compressive strain.The band offsets calculated using Equation (2.26-28) (shown in Figure 3.27) exhibit some important characteristics.

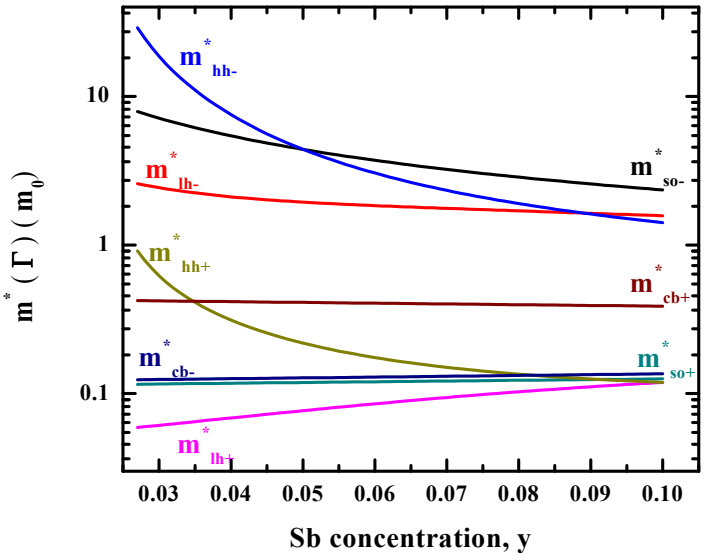

Figure 3.32 Effective masses $m^*(\Gamma)$ of the electrons and holes in the upper and lower conduction and valence sub bands versus Sb concentration along Σ direction.

CBO increases at a rapid rate with Sb and N concentration unlike the LH and HH related band offsets. CBO, which shows a non-linear increase, is almost ten times greater than the LH and HH band offsets increasing linearly. While the band offset ΔE_{hh} decreases with the increase in N and Sb concentration, ΔE_{lh} decreases. This is due to the opposite effect of the shearing component of strain on HH and LH bands as can be observed from Equation (2.26-28).

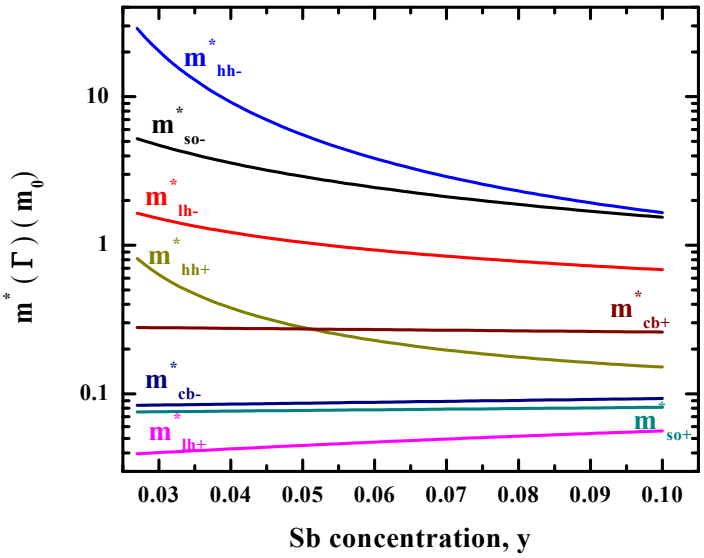

Figure 3.33 Effective masses $m^*(\Gamma)$ of the electrons and holes in the upper and lower conduction and valence sub bands versus Sb concentration in the crystal direction Λ.

The effective masses for tensile strained GaAsSbN/GaAs QWs depicted in Figure 3.28, Figure 3.29 and Figure 3.30 along three highly symetric direction Δ, Σ and Λ respectively, which clearly reveals that the carrier effective masses m^*_{cb-}, m^*_{hh+}, m^*_{lh+} and m^*_{so+} have values lesser than the free electron effective mass m_0. The effective masses m^*_{cb-} m^*_{hh+} m^*_{lh+} and m^*_{so+} decrease with the increase in N concentration for compressive strained GaAsSbN/GaAs QWs. The effective masses for compressive strained GaAsSbN/GaAs QW depicted in Figure 3.31, Figure 3.32 and Figure 3.33 along three highly symetric direction Δ, Σ and Λ respectively, which clearly reveals that the carrier effective masses m^*_{cb-}, m^*_{hh+}, m^*_{lh+} and m^*_{so+} have values lesser than the free electron effective mass m_0. While the effective masses m^*_{cb-} m^*_{lh+} and m^*_{so+} increase with the increase in Sb concentration, m^*_{hh+} decreases for compressive strained GaAsSbN/GaAs QWs. The

decrease in effective masses can be associated with the corresponding increase in mobility for the CB electrons and HH and SO holes and thus can be utilized for the fabrication of optoelectronic devices with superior carrier transport properties.

3.2 Optical Properties

Considering band offsets, carrier effective masses and band structures from corresponding **k.p** Hamiltonian we have calculated optical properties of GaSbBi/GaAs and GaAsSbN/GaAs QW structures for numerous application in optoelectronic devices.

3.2.1 Optical Properties of GaSbBi

Collecting corresponding band offsets from 14×14 system Hamiltonian of GaSbBi/GaAs QW we have calculated the following optical properties.

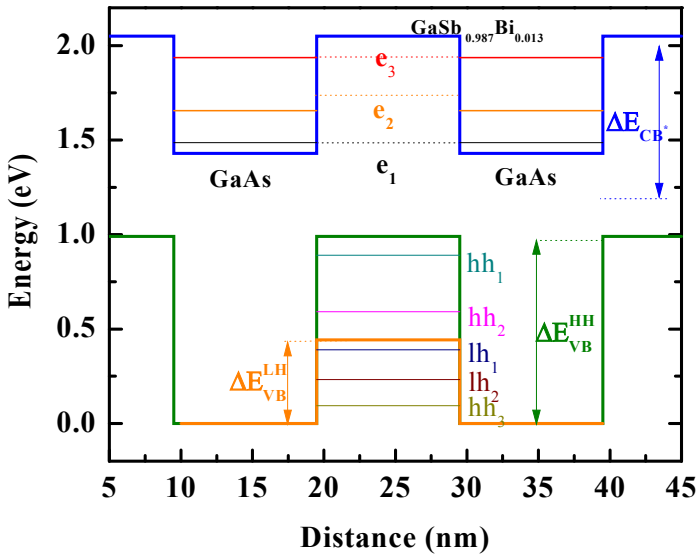

Figure 3.34 Confinement potential energy levels of 10 nm width $GaSb_{0.987}Bi_{0.013}$/GaAs type-II QW.

One of the significant parameters for the calculation of optical gain is the band offset which is obtained using Equation (2.26-28). Figure 3.34 shows the Type II band structure of a 10 nm wide $GaSb_{0.987}Bi_{0.013}$/GaAs QWs in accordance with [17]. The different excited energy states for heavy hole, light hole and conduction band electrons are also depicted in the figure. The large values of HH, LH and CB offsets of 0.99 eV, 0.4425 eV and 0.62 eV respectively results in higher confinement potential of both the electrons and holes in the CB and VB. Substantial refractive index difference between GaSb and GaAs and higher values of band offsets provide better optical and carrier confinement that leads to the enhancement of lasing action for GaSbBi/GaAs QW structures. Moreover, unlike Type I band structure in GaAsBi/GaAs QWs, Type II structure in GaSbBi/GaAs QWs offers higher overlap between electron and hole wave function which

improves the density of state and owing to higher carrier accumulation luminosity of the optoelectronic devices improve for Type II QWs [70]. Moreover, lesser amount of compressive strain (7%) due to dilute Bi concentration helps to achieve longer emission wavelength with larger material gain in GaSbBi/GaAs QWs.

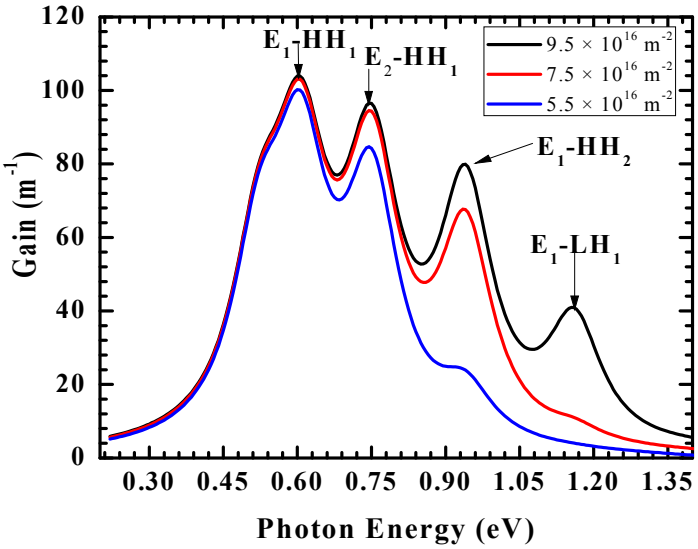

Figure 3.35 Plot of Gain versus Photon energy for different carrier concentrations showing the Interband transitions in GaAsBi/GaAs QWs.

Figure 3.35Figure 3.35 shows the plot of gain as a function of energy for different injected carrier concentrations. The gain curve exhibits four peaks which can be interpreted as the interband transitions occurring between the excited HH/LH and conduction sub bands calculated from Figure 3.34.

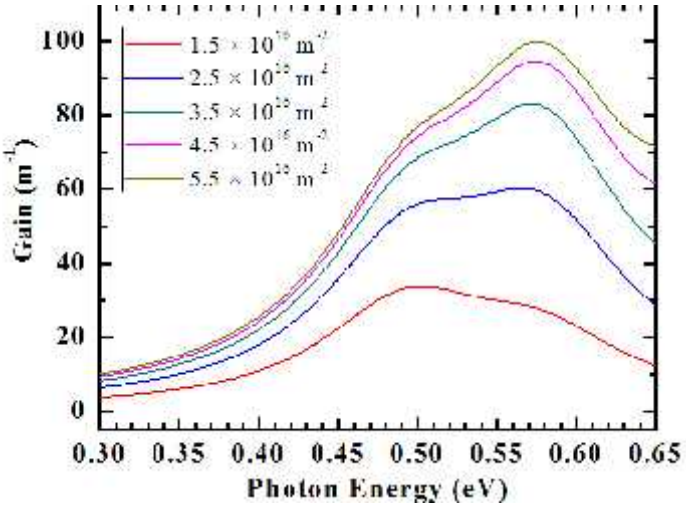

Figure 3.36 Optical gain spectra of 10 nm width $GaSb_{0.987}Bi_{0.013}$/GaAs QW calculated within 14-band k.p model for various carrier concentrations.

As the carrier concentration decreases, peaks 3 and 4 depicting the transition between conduction sub band and HH and LH sub bands respectively fade away. We have also calculated the values of intersubband transitions occurring between the heavy hole and light hole energy bands. The transitions from a HH to a LH state is important from the point of view of absorption of normally incident light by holes in GaAs based p-Quantum Well Infrared Photodetecors (QWIP) in the absence of an optical grating [71].

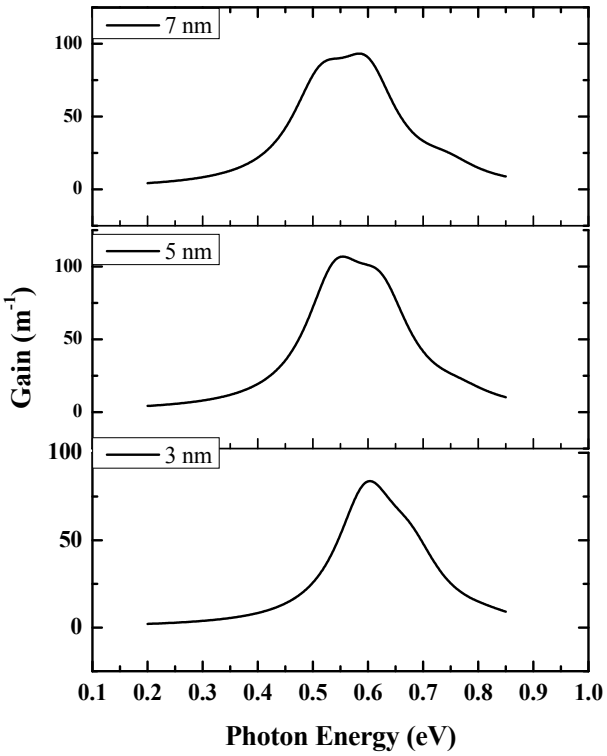

Figure 3.37 Optical gain spectra of $GaSb_{0.987}Bi_{0.013}/GaAs$ QW for various widths calculated within 14-band k.p model for carrier concentration of 3×10^{16} m^{-2}.

The inter subband transitions in the Conduction Band ranges from 0.17-0.45 eV whereas the transitions between the LH→HH/HH→HH/LH→LH subbands lie in the range 0.14-0.80 eV. It has been found out numerically that the hole intersubband absorption of normally incident radiation in the absence of an optical grating would be largest for transitions from a pure heavy hole state to a pure light hole state [72]. The sub band energy levels, effective masses and band offsets are used to calculate the optical gain with respect to the inter subband transitions.

Figure **3.36** shows the shift of the peak of optical gain with the variation in injected surface carrier density of the $GaSb_{0.987}Bi_{0.013}/GaAs$ QW with 10 nm active layer. Increasing the rate of injected carrier density improves the difference between the Fermi function which leads to gain improvement within the desired mid infrared

region. For quantum confined structures like QWs, the sub bands act as a tuning parameter for optoelectronic devices. The variation of the confinement length of the QWs causes variation in the sub bands E_n^c and E_m^v which leads to change in effective band gap of QWs and changes the peak gain position. We have analyzed the confinement effect on optical gain for a surface carrier density of 3×10^{16} m^{-2} which is shown in Figure 3.37.

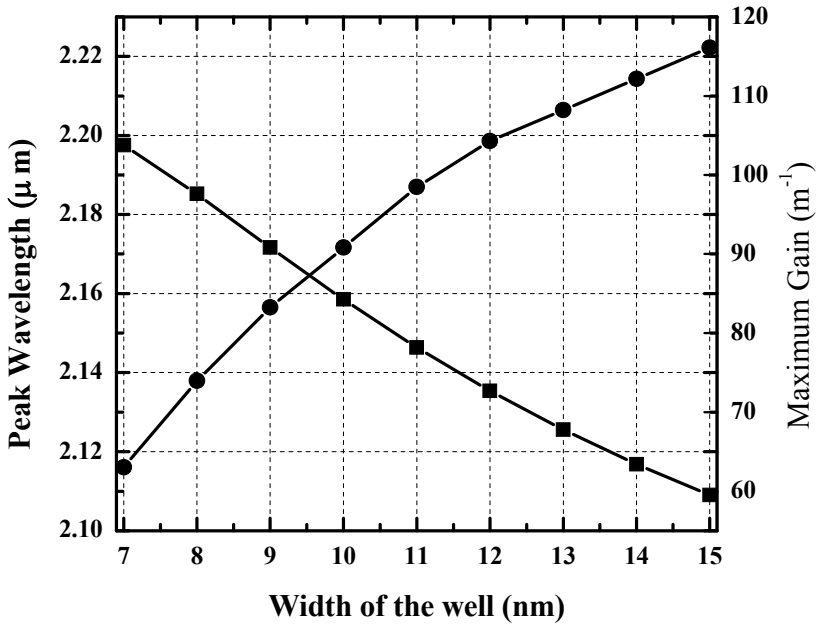

Figure 3.38 Peak gain and corresponding peak wavelength of of $GaSb_{0.987}Bi_{0.013}$/GaAs QW for various widths calculated within 14-band k.p model for carrier concentration of 3×10^{16} m^{-2} .

Reducing the dimension of the active region of the QWs causes a shift of the peak energy position towards lower wavelengths for a constant injected carrier density and this occurs due to the inverse squared dependence of the energy of the sub bands on the width of the QWs. Stronger confinement of the carriers due to the overlap of the exciton wave functions increases the transition energy for the carriers which shifts of the peak of gain towards lower wavelengths which is shown in Figure 3.37. Figure 3.38 depicts the opposite characteristics of the optical gain and peak energy position with the dimension of the QWs.

3.2.2 Optical Properties of GaAsSbN

Considering corresponding band offsets from 16×16 system Hamiltonian of GaAsSbN/GaAs QW we have calculated the following optical properties.

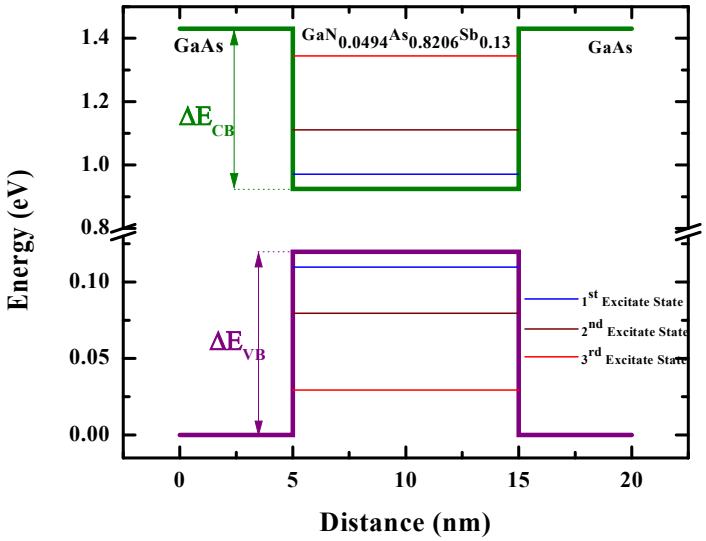

Figure 3.39 The quantum confinement potential and energy levels for electrons and holes for a set of 10 nm wide GaAsNSb/GaAs QWs for lattice matched condition.

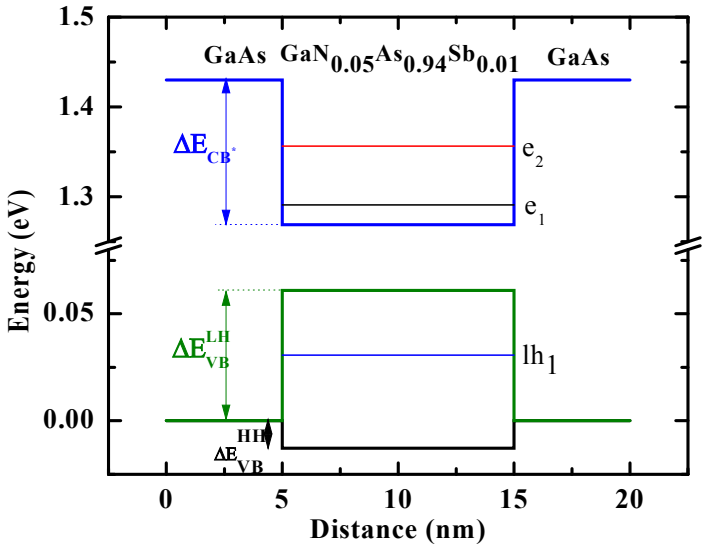

Figure 3.40 The quantum confinement potential and energy levels for electrons and holes for a set of 10 nm wide GaAsNSb/GaAs QWs for tensile strain.

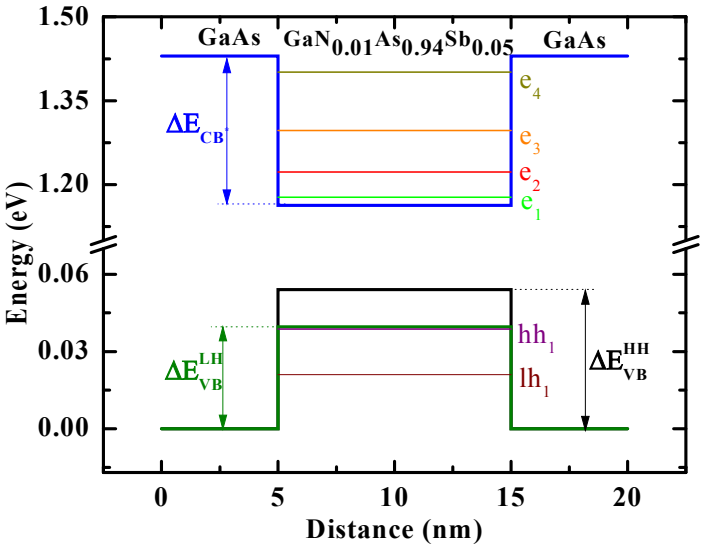

Figure 3.41 The quantum confinement potential and energy levels for electrons and holes for a set of 10 nm wide GaAsNSb/GaAs QWs for compressive strain.

Figure 3.39, Figure 3.40 and Figure 3.41 shows the quantum confinement potential and the positions of the VB and CB energy levels for lattice matched, tensile strained and compressive strained 10 nm wide GaAsNSb/GaAs QWs. The dispersion of the energy levels in both the CB and VB increases significantly in compressive strained QWs. Hence, longer emission wavelengths in the telecommunication window (1.3-1.55 μm) can be achieved for $GaAs_{0.94}N_{0.01}Sb_{0.05}$/GaAs QWs. Clearly, the figures show that GaAsNSb/GaAs QWs are Type I structures with strong confinement potential for both holes and electrons.

Table 4 Operating wavelength range in μm

Bulk		Tensile		Compressive	
High	Low	High	Low	High	Low
1.44	0.95	1.62	0.9	1.343	0.91

4 Conclusion and Future Work

A mathematical model based on VBAC is used to calculate the electronic band structures of $GaSb_{1-x}Bi_x$ for x= 0.013 along the <100> and <111> both for bulk and strained layer grown on GaAs. VBAC model predicts that for an incorporation of 1.3% Bi in GaSb conduction band minima is pushed downward by 36 meV and the valance band maxima is shifted upward by 15 meV which produces a band gap reduction of 51 meV. The splitting of the LH and HH bands and the upward shift of the CB results in a huge band gap of 1.12 eV for GaSbBi/GaAs QWs. The separation of the LH and HH bands by about 373 meV is mainly due to the generation of strain for the large lattice mismatch between GaSbBi and GaAs. The downward shift of the spin-orbit split-off band E_{SO+} by 230 meV increases the spin-orbit splitting energy. The carrier confinement and strain immensely also affects the CB shifting it by 0.66 eV with respect to the CB of GaSb. The calculated dispersion relations show that E_{so+} is isotropic in all orientation of **k** upto k=0.10 $Å^{-1}$ and E_{cb-} and E_{so-} reflects a moderate change with **k**-direction beyond the value of k=0.12 $Å^{-1}$ unlike $E_{hh/lh\pm}$ bands. The increase in the effective masses of the charge carriers is also due to the confinement of electrons in the QW structure. The carrier effective masses m^*_{hh+}, m^*_{lh+} and m^*_{so+} in the upper sub bands are almost isotropic. The large values of HH, LH and CB offsets for GaSbBi/GaAs QWs results in higher confinement potential of both the electrons and holes in the CB and VB. The optical gain of the QWs increase with an increase of the injected carrier charge density. However, the increase in the dimension of the QWs reduces the optical gain for a constant injection carrier density due to the reduction in the density of the states in the sub bands. The peak of the optical gain curve exhibits a blueshift due to the reduction in the width of the QWs.

GaSbBi/GaAs QW systems are suited for applications in optoelectronic devices due to the innumerous advantages that these systems provide. Firstly, GaSbBi has a large spin orbit splitting energy and incorporation of a few percent of Bi results in the formation of $\Delta_{SO}>E_g$ regime for low temperatures which is not only vital for spintronic applications but it also inhibits the Auger recombination losses that degrades the efficiency of LASERs. Secondly, Bi perturbs only the valence band of GaSb and hence the electron mobility remains unaffected. This improves the speed response and sensitivity of GaSbBi/GaAs based photodetectors.

The enhanced optical as well as carrier confinement of GaSbBi/GaAs QWs improves the lasing action of such systems to a great extent. The inter sub band transitions occurring in GaSbBi/GaAs QWs, mainly between the HH and LH sub bands allows normal incidence inter subband absorption in p-QWIPs in the absence of an optical grating. Moreover the inter subband transitions occurring between the VB and CB sub bands could make possible the fabrication of LASER diodes operating in the 1.5-2.2 μm mid-infrared region.

We have calculated the band structure of GaAsNSb alloys lattice matched to GaAs substrates and GaAsNSb/GaAs QWs using a 16 band k·p Hamiltonian. Our calculations show that a significant band gap reduction of 330 meV is obtained for $GaAs_{0.931}N_{0.019}Sb_{0.05}$ alloys lattice matched to GaAs. The spin-orbit splitting energy increases at the rate of 22meV/%Sb resulting in a crossover with the band gap energy E_g for Sb = 27% and N = 10% and a resonant energy of 0.44 eV. Hence GaAsNSb alloys with a spin-orbit splitting energy larger than the band gap can be used to design potential Auger and leakage free devices operating in the long wavelength regime. Calculation of effective masses indicate that unlike the dilute nitrides, the electron mobility in GaAsNSb alloys increases for y>3% and the hole mobility decreases with the increase in Sb concentration. VBO and CBO as well their ratios are calculated as function of both Sb and N mole fraction. CBO as high as 500 meV and VBO of 120 meV is obtained which can improve the device characteristics by providing strong carrier confinement. Band gap values of 0.75 eV and 1.22 eV are obtained for tensile strained $GaAs_{0.94}N_{0.05}Sb_{0.01}$/GaAs QW and compressive strained $GaAs_{0.94}N_{0.01}Sb_{0.05}$/GaAs QWs respectively. The splitting between LH and HH sub bands are observed in case of tensile strained QWs. For QWs, CBO shows a non-linear increase and is almost ten times greater than the LH and HH related VBO. The effective masses m^*_{cb-} m^*_{hh+} and m^*_{so+} decrease with the increase in Sb concentration, m^*_{lh+} increases for compressive strained GaAsSbN/GaAs QWs in the crystal direction [100]. It is also shown that it is possible to achieve emission at telecommunication windows (i.e., 1.3 μm and 1.55 μm) for GaAs-based lasers containing GaAsNSb/GaAs QWs.

In future we would like to investigate the optoelectronic devices like Photo detector, LASER diode and Solar cell by using our investigated materials GaSbBi and GaAsSbN. The detailed device simulation and fabrication would help to enrich and support our recent work.

Bibliography

[1] D. P. Samajdar, T. D. Das, and S. Dhar, Mater. Sci. Semicond. Process. **40,** 539 (2015).

[2] K. Alberi, J. Wu, W. Walukiewicz, K. M. Yu, O. D. Dubon, S. P. Watkins, C. X. Wang, X. Liu, Y.-J. Cho, and J. Furdyna, Phys. Rev. B **75**, 045203 (2007).

[3] M. P. Polak *et al.* J. Phys. D: Appl. Phys. **47,** 355107 (2014).

[4] M. P. Polak, P. Scharoch, R. Kudrawiec, Semicond. Sci. Technol. **30,** 094001 (2015).

[5] D. P. Samajdar and S. Dhar, Superlattices Microstruct. **89,** 112 (2016).

[6] S. K. Das, T. D. Das, S. Dhar, M. de la Mare, A. Krier, Infrared Phys. Technol. **55,** 156-160 (2012).

[7] S. K. Das, T. D. Das, S. Dhar, Semicond. Sci. Technol. **29,** 015003 (2014).

[8] M. K. Rajpalke, W. M. Linhart, M. Birkett, K. M. Yu, J. Alaria, J. Kopaczek, R. Kudrawiec, T. S. Jones, M. J. Ashwin, T. D. Veal, J. Appl. Phys. **116,** 043511 (2014).

[9] M. K. Rajpalke *et al.* App. Phys. Lett. **103,** 142106 (2013).

[10] S. Y. Lin *et al.* Appl. Phys. Lett. **96 ,** 123503 (2010).

[11] M. Geller, C. Kapteyn, L. Müller-Kirsch, R. Heitz, D. Bimberg, Appl. Phys. Lett. **82,** 2706 (2003).

[12] A. Marent *et al.* Appl. Phys. Lett. **89,** 072103 (2006).

[13] J. Hwang, A. J. Martin, J. M. Millunchick, J. D. Phillips, J. Appl. Phys. **111**, 074514 (2012).

[14] S. Y. Lin *et al.* Appl. Phys. Lett. **96,** 123503 (2010).

[15] H. Zhao, R. A. Arif, N. Tansu, J. Appl. Phys. **104**, 043104 (2008).

[16] R.A. Arif, H. Zhao, Y. K. Ee, N. Tansu, IEEE J. Quantum Electron. **44,** 573 (2008).

[17] T. D. Das, D. P. Samajdar, M. K. Bhowal, S. C. Das, and S. Dhar, Curr. Appl. Phys. **16,** 1615 (2016).

[18] S. A. Lourenco, I. F. L. Dias, J. L. Duarte, E. Laureto, V. M. Aquino, and J. C. Harmand, Braz. J. Phys. 37, 1212 (2007).

[19] Y-T. Lin, T-C. Ma, T-Y. Chen, and H-H. Lin, Appl. Phys. Lett. **93**, 171914 (2008).

[20] T. D. Veal, L. F. J. Piper, S. Jollands, B. R. Bennett, P. H. Jefferson, P. A. Thomas, C. F. McConville, B. N. Murdin, L. Buckle, G. W. Smith, T. Ashley, Appl. Phys. Lett. 87 132101 (2005).

[21] J. C. Harmand, A. Caliman, E. V. K Rao, L. Largeau, J. Ramos, R. Teissier, L. Travers, G. Ungaro, B. Theys and I. F. L. Dias, Semicond. Sci. Technol. **17** 778 (2002).

[22] G. Ungaro, Le Roux, R. Teissier, J. C. Harmand, Electron. Lett. 35 15 (1999).

[23] J. C. Harmand, G. Ungaro, J. Ramos, E. V. K. Rao, G. Saint-Girons, R. Teissier, G. Le Roux, L. Largeau, and G. Patriarche, J. Cryst. Growth 227 553 (2001).

[24] Aymeric Maros, Nikolai Faleev, Richard R. King, and Christiana B. Honsberg, J. Vac. Sci. Technol. B **34**, 02L106 (2016).

[25] J. C. Harmand, L. Largeau, and F. Glas, Phys. Stat. Sol. C **3** 1931 (2006).

[26] P. Kasanaboina, M. Sharma, P. Deshmukh, C. L. Reynolds Jr., Y. Liu and S. Iyer, Nanoscale Res. Lett. 11, 47 (2016).

[27] J. Bardeen, J. Chem. Phys. **6**, 367 (1938).

[28] F. Seitz, *The Modern Theory of Solids*, McGraw-Hill, New York, 1940.

[29] W. Shockley, Phys. Rev. **78**, 173-174, (1950).

[30] G. Dresselhaus, A. F. Kip, and C. Kittel, Phys. Rev. **98**, 368-384, (1955).

[31] E. O. Kane, J. Phys. Chem. Solids **1**, 249-261, (1957).

[32] E. O. Kane, in *Semiconductor and Semimetals*, edited by R. K. Willardson and A. C. Beer (Academic Press, New York, 1966).

[33] J. M. Luttinger and W. Kohn, Phys. Rev. **97**, 869-883 (1955).

[34] J. M. Luttinger, Phys. Rev. **102**, 1030-1041 (1956).

[35] The k·p Method: Electronic Properties of Semiconductors, in: Lok C. Lew Yan Voon, M. Willatzen, Springer, Springer-Verlag Berlin Heidelberg, New York, 2009.

[36] S. T. Ng, W. J. Fan, Y. X. Dang, S. F. Yoon, Phys. Rev. B **72,** 115341 (2005).

[37] I. Vurgaftman, J.R. Meyer, L.R. Ram-Mohan, J. Appl. Phys. **89,** 5815 (2001).

[38] D.P. Samajdar, Utsa Das, A.S. Sharma, S. Das and S. Dhar, Curr. Appl. Phys. **16,** 1687 (2016).

[39] D. P. Samajdar and S.Dhar, The Sci. World. J. *2014* 704830 (2014).

[40] M. M. Habchi, A. Ben Nasr, A. Rebey, B. El Jani, Infrared Phys. Tech. **61,** 88 (2013).

[41] Z-G. Song, S. Bose, W-J. Fan, and S-S. Li, J. Appl. Phys. **119**, 143103 (2016).

[42] G. L. Bir and G. E. Pikus, Symmetry and Strain-Induced Effects in Semiconductors Wiley, New York, 1976.

[43] G. M. T. Chai *et al.*, Semicond. Sci. Technol. **3,** 94015 (2015).

[44] M. Ferhat, A. Zaoui, Phys. Rev. B - Condens. Matter Mater. Phys. **73,** 1 (2006).

[45] S. Nacer, A. Aissat, and K. Ferdjani, Opt. Quantum Electron. **40**, 677 (2008).

[46] R. Kudrawiec, J. Kopaczek, M. P. Polak, P. Scharoch, M. Gladysiewicz, J. Misiewicz,

R. D. Richards, F. Bastiman, and J. P. R. David, J. Appl. Phys. **116**, 0 (2014).

[47] S. L. Chuang, Physics of Optoelectronic Devices (Pure and Applied Optics). New York, NY, USA: Wiley, 1995.

[48] W. W. Chow and S. W. Koch, Semiconductor-Laser Fundamentals: Physics of the Gain Materials. New York, NY, USA: Springer-Verlag,1999.

[49] A. Ben Ahmed, H. Saidi, S. Ridene, and H. Bouchriha, IEEE J. Q. E. **51**, 1 (2015).

[50] M. Debbichi *et al.*, Semicond. Sci.Technol., **24** 085010-1 (2009).

[51] V. V Lysak, H. Kawaguchi, and I.A. Sukhoivanov, IEEE Proc. Opto. **152**, 131 (2005).

[52] M. Asada, A. Kameyama and Y. Suematsu, IEEE J. Quantum Electron. **20,** 745 (1984).

[53] C. G. Van de Walle, Phys. Rev. *B* **39,** 1871 (1989).

[54] B. Chen, IEEE Trans. Electron Dev **64,** 1606 (2017).

[55] K. K. Nagaraja, Y. A. Mityagin, M. P. Telenkov, I. P. Kazakov, Crit. Rev. Solid State Mater. Sci. **0,** 1 (2016).

[56] H. Tong, X. Marie, and M. W. Wu, J. Appl. Phys. **112,** 063701(2012).

[57] L. F. Bian, D. S. Jiang, P. H. Tan, S. L. Lu, B.Q. Sun, L. H. Li, J. C. Harmand, Solid State Commun. **132**, 707 (2004).

[58] F. Bousbih, S.B. Bouzid, R. Chtourou, F.F. Charfi, J.C. Harmand, G. Ungaro, Mater. Sci. Eng. C **21,** 251 (2002).

[59] L. Malikova, F. H. Pollak and R. Bhat, Journal of Elec. Mater. **27** 484 (1998).

[60] K. Uesugi K, N. Marooka and I. Suemune , Appl. Phys. Lett.**74** 1254 (1999).

[61] R. Bhat, C. Caneau, L. S. Riba, W. Bi and C. Tu J. Cryst. Growth **195,** 427 (1998).

[62] B. M. Keyes, J. F. Geisz, P. C. Dippo, R. Reedy, C. Kramer, D. J. Friedman, R. S. Kurtz and J. M. Olson, NCPV Photovoltaics Program Review *AIP Conf. Proc.* **462** 511(1999).

[63] G. A. Antypas and L. W. James, J. Appl. Phys. **41,** 2165 (1970).

[64] R. E. Nahory, M. A. Pollack, J. C. DeWinter, and K. M. Williams, J. App. Phys. 48, 1607 (1977).

[65] Y. Mitsuaki, S. Yukio, I. Tetsuo, M. Yuichi and K. Morihiko, Jpn. J. Appl. Phys. **17** 2091(1978).

[66] A. E. Taylor and E. Fortin, Can. J. Phys. 48, 1874 (1970).

[67] G. Ungaro, I. Sagnes, G. Le Roux, L. Largeau, G. Patriarche, J. Saint-Girons, and J.C. Harmand, Conf. Proceedings. 2000 Int. Conf. Indium Phosphide Relat. Mater. (Cat. No.00CH37107) 553 (2000).

[68] H.-P. Hsu, Y.-T. Lin and H.-H. Lin, Jpn. J. Appl. Phys. **51**, 022605 (2012).

[69] R.N. Kini, A.J. Ptak, B. Fluegel, R. France, R.C. Reedy, A. Mascarenhas, Phys. Rev. B **83,** 075307(2011).

[70] S. Mazzucato, T. Zhang, H. Carrere, D. Lagarde, P. Boonpeng, A. Arnoult, G. Lacoste, A. Balocchi, A. Amand, C.Fontaine, and X. Marie, Appl. Phys. Lett. **102,** 252107 (2013).

[71] J. L. Pan and C. G. Fonstad, Jr., IEEE Trans. Electron Dev. **47,** 1325 (2000).

Annexure I : List of Publications

Journals:

1. "*Effect of Sb and N resonant states on the band structure and carrier effective masses of GaAs1-xyNxSby alloys and GaAs1-x-yNxSby/GaAs quantum wells calculated using k·p Hamiltonian*" **Indranil Mal**, D. P. Samajdar and T. D. Das, Superlattices and Microstructures, 106, 20-32 (2017).
2. "*Calculation of Band Structure and Optical Gain of Type-II GaSbBi/GaAs Quantum Wells Using 14-Band k•p Hamiltonian*" **Indranil Mal**, D. P. Samajdar and T. D. Das, Superlattices and Microstructures, in Press (2017).

Annexure II : Reprint of Publications

ELSEVIER LICENSE
TERMS AND CONDITIONS

May 19, 2017

This Agreement between Indranil Mal ("You") and Elsevier ("Elsevier") consists of your license details and the terms and conditions provided by Elsevier and Copyright Clearance Center.

License Number	4112281437409
License date	May 19, 2017
Licensed Content Publisher	Elsevier
Licensed Content Publication	Superlattices and Microstructures
Licensed Content Title	Effect of Sb and N resonant states on the band structure and carrier effective masses of GaAs1-x-yNxSby alloys and GaAs1-x-yNxSby/GaAs quantum wells calculated using k·p Hamiltonian
Licensed Content Author	Indranil Mal,D.P. Samajdar,T.D. Das
Licensed Content Date	June 2017
Licensed Content Volume	106
Licensed Content Issue	n/a
Licensed Content Pages	13
Start Page	20
End Page	32
Type of Use	reuse in a thesis/dissertation
Portion	full article
Format	print
Are you the author of this Elsevier article?	Yes
Will you be translating?	No
Order reference number	
Title of your thesis/dissertation	STUDIES ON III-V DILUTE NITRIDE, BISMUTH AND ANTIMONIDE III-V ALLOYS USING K.P HAMILTONIAN
Expected completion date	May 2017
Estimated size (number of pages)	60
Elsevier VAT number	GB 494 6272 12
Requestor Location	Indranil Mal 23/19 jessore road, kolkata kolkata, 700028 India Attn: Indranil Mal
Total	0.00 USD
Terms and Conditions	

INTRODUCTION

1. The publisher for this copyrighted material is Elsevier. By clicking "accept" in connection with completing this licensing transaction, you agree that the following terms and conditions apply to this transaction (along with the Billing and Payment terms and conditions

Superlattices and Microstructures 106 (2017) 20–32

Contents lists available at ScienceDirect

Superlattices and Microstructures

journal homepage: www.elsevier.com/locate/superlattices

Effect of Sb and N resonant states on the band structure and carrier effective masses of $GaAs_{1-x-y}N_xSb_y$ alloys and $GaAs_{1-x-y}N_xSb_y$/GaAs quantum wells calculated using k·p Hamiltonian

Indranil Mal [a], D.P. Samajdar [b, *], T.D. Das [c]

[a] Department of Electronics and Computer Engineering, National Institute of Technology, Arunachal Pradesh 791112, India
[b] Department of Electronics & Communication Engineering, Heritage Institute of Technology, Kolkata 700107, India
[c] Department of Basic & Applied Science, National Institute of Technology, Arunachal Pradesh 791112, India

ARTICLE INFO

Article history:
Received 17 February 2017
Received in revised form 21 March 2017
Accepted 22 March 2017
Available online 26 March 2017

ABSTRACT

GaAsNSb is a promising candidate for use in GaAs-based optoelectronic devices in the 1.33 −1.55 μm wavelength region. We have calculated the band structure of dilute nitride-antimonide $GaAs_{1-x-y}N_xSb_y$ alloys, lattice matched to GaAs, using Band anticrossing (BAC) and Valence Band Anticrossing (VBAC) model in conjugation with **k·p** Hamiltonian method. This mathematical model in the form of a 16 band Hamiltonian matrix is used to examine the shift of different bands as a function of Sb concentration for both bulk and quantum well structures for GaAsNSb/GaAs. The band parameters such as energy gap, spin-orbit splitting energy, carrier effective masses, band offsets, and strain generated due to the growth of GaAsNSb/GaAs heterostructures as a function of Sb and N concentrations are calculated and compared with the recent experimental data. The substitution of As atoms due to the incorporation of N and Sb impurity atoms causes a significant band gap reduction of ~330 meV for $GaAs_{0.971}Sb_{0.015}N_{0.019}$ alloys. The enhancement of spin-orbit splitting energy causes a crossover between E_g and Δ_{so} for Sb and N concentration of 27 and 10 at % respectively. Suitable tuning of the band offset values with Sb and N concentrations makes GaAsNSb/GaAs alloy system an efficient alternative for band gap engineering and fabricating photonic device structures.

1. Introduction

Dilute III-V Nitride alloys have attracted the attention of the researchers in the past few decades due to their unique physical properties such as simultaneous reduction of band gap and lattice parameter of the corresponding III-V host lattice and potential applications in GaAs-based optoelectronic and photonic devices operating in the strategically important telecommunication wavelength range of 1.3–1.55 μm [1–4]. GaAsNSb is a favourable alternative for achieving longer wavelengths with lower N concentration compared to GaInAsN [5]. Smaller value of energy band gap is achievable with GaAsNSb than with GaInAsN for the same nitrogen concentration as GaAsSb presents a stronger bandgap bowing than GaInAs [6]. Harmand and co workers reported a band gap reduction of 180 meV for a nitrogen incorporation of 1% in GaAsNSb/GaAs quantum wells (QWs) [4–6]. Though GaAsNSb (QW) structures are not suitable for the fabrication of

* Corresponding author.
E-mail address: dipprakash010@gmail.com (D.P. Samajdar).

http://dx.doi.org/10.1016/j.spmi.2017.03.035
0749-6036/

ELSEVIER ORDER DETAILS

May 19, 2017

Order Number	501271285
Order date	May 19, 2017
Licensed Content Publisher	Elsevier
Licensed Content Publication	Superlattices and Microstructures
Licensed Content Title	Calculation of band structure and optical gain of type-II GaSbBi/GaAs quantum wells using 14-band k·p Hamiltonian
Licensed Content Author	Indranil Mal,D.P. Samajdar,T.D. Das
Licensed Content Date	Available online 16 May 2017
Licensed Content Volume	n/a
Licensed Content Issue	n/a
Licensed Content Pages	1
Start Page	
End Page	
Type of Use	reuse in a thesis/dissertation
Intended publisher of new work	other
Portion	full article
Format	print
Are you the author of this Elsevier article?	Yes
Will you be translating?	No
Order reference number	
Title of your thesis/dissertation	STUDIES ON III-V DILUTE NITRIDE, BISMUTH AND ANTIMONIDE III-V ALLOYS USING K.P HAMILTONIAN
Expected completion date	May 2017
Estimated size (number of pages)	60
Elsevier VAT number	GB 494 6272 12
Requestor Location	Indranil Mal 23/19 jessore road, kolkata kolkata, 700028 India Attn: Indranil Mal
Total	Not Available

Superlattices and Microstructures

Available online 16 May 2017

In Press, Accepted Manuscript — Note to users

Calculation of Band Structure and Optical Gain of Type-II GaSbBi/GaAs Quantum Wells Using 14-Band k·p Hamiltonian

Indranil Mal[1], D.P. Samajdar[2], T.D. Das[3]

[1] Department of Electronics and Computer Engineering, National Institute of Technology, Arunachal Pradesh 791112, India

[2] Department of Electronics & Communication Engineering, PDPM Indian Institute of Information Technology, Design and Manufacturing, Jabalpur, Madhya Pradesh-482005, India

[3] Department of Basic & Applied Science, National Institute of Technology, Arunachal Pradesh 791112, India

Available online 16 May 2017

Show less

https://doi.org/10.1016/j.spmi.2017.05.032

Highlights:

- Band structure of GaSbBi/GaAs quantum wells (QWs) calculated.
- Generation of strain splits LH and HH sub bands
- GaSbBi/GaAs QDs exhibit indirect gap type-II band alignment
- Optical gain of GaSbBi/GaAs (QWs) depends on width of the well
- Peak of the gain curve exhibits a shift towards lower wavelengths

***Abstract*—** The electronic band structure of strained GaSbBi/GaAs heterostructures are investigated using a 14 band k·p Hamiltonian which is an extended form of the 12 band Valance band Anticrossing (VBAC) matrix. The shift in the valence and conduction sub bands due to the incorporation of Bi in GaSb/GaAs Type II system are calculated and compared with the available experimental data. Unlike the band gap reduction of 51 meV and enhancement of spin-orbit splitting energy by ~ 27 meV in bulk $GaSb_{0.987}Bi_{0.013}$, 7.3% compressive strain in GaSbBi/GaAs quantum wells (QWs) amends the scenario completely by increasing the band gap to 1.12 eV and the spin-orbit splitting energy to 1.217 eV. The dispersion relations and effective masses of the carriers in the crystal directions Δ, Λ and Σ are calculated near the Γ point using this Hamiltonian yield some interesting results. The variation of the optical gain with the density of injected carriers and dimension of the QW is calculated and the peak of the gain curve exhibits a shift towards lower wavelengths with the decrease in the width of the QWs.

Keywords

VBAC; GaSbBi/GaAs; Quantum wells; k·p method; compressive strain; band gap